

Journal Pre-proof

A modal discontinuous Galerkin method for simulating dusty and granular gas flows in thermal non-equilibrium in the Eulerian framework

Omid Ejtehad, R.S. Myong

PII: S0021-9991(20)30184-4
DOI: <https://doi.org/10.1016/j.jcp.2020.109410>
Reference: YJCPH 109410

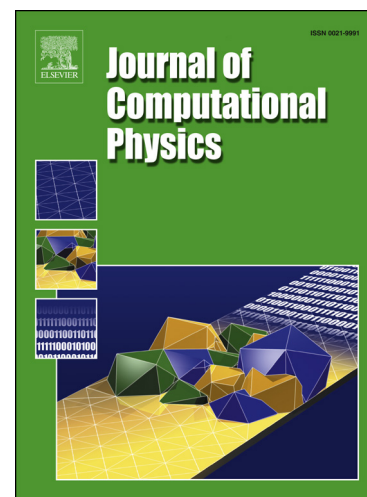
To appear in: *Journal of Computational Physics*

Received date: 29 November 2019
Revised date: 11 March 2020
Accepted date: 16 March 2020

Please cite this article as: O. Ejtehad, R.S. Myong, A modal discontinuous Galerkin method for simulating dusty and granular gas flows in thermal non-equilibrium in the Eulerian framework, *J. Comput. Phys.* (2020), 109410, doi: <https://doi.org/10.1016/j.jcp.2020.109410>.

This is a PDF file of an article that has undergone enhancements after acceptance, such as the addition of a cover page and metadata, and formatting for readability, but it is not yet the definitive version of record. This version will undergo additional copyediting, typesetting and review before it is published in its final form, but we are providing this version to give early visibility of the article. Please note that, during the production process, errors may be discovered which could affect the content, and all legal disclaimers that apply to the journal pertain.

© 2020 Published by Elsevier.



Highlights

- A modal DG method for computing rarefied gaseous flows interacting with rigid particles and granular medium is presented.
- Full continuum models based on a two-fluid model can cover a wide range of gas and solid phase regimes.
- A high-fidelity approach is developed to treat the non-strictly hyperbolic equations of a dusty gas.
- The computational model is used to simulate the impingement of an underexpanded jet on a dusty surface in a rarefied condition.

Journal Pre-proof

**A modal discontinuous Galerkin method for simulating dusty
and granular gas flows in thermal non-equilibrium
in the Eulerian framework**

Omid Ejtehadi ^{a,b}, R. S. Myong^{a*}

^a *School of Mechanical and Aerospace Engineering, and ACTRC & ReCAPT, Gyeongsang
National University, Jinju, Gyeongnam 52828, South Korea*

^b *Supercomputing Modeling and Simulation Center, Korea Institute of Science and
Technology Information (KISTI), Daejeon 305-806, South Korea*

**Corresponding author: Tel +82 55 772 1645 (Fax 1580); myong@gnu.ac.kr*

Abstract

A modal discontinuous Galerkin method was developed for computing compressible rarefied gaseous flows interacting with rigid particles and granular medium. In contrast to previous particle-based models that were developed to handle rarefied flows or solid phase particles, the present computational method employs full continuum-based models. This work is one of the first attempts to apply the modal discontinuous Galerkin method to a two-fluid model framework, which covers a wide range of gas and solid phase regimes, from a continuum to non-equilibrium gas, and from dusty to collisional regimes. The rarefaction effects were taken into account by applying the second-order Boltzmann-Curtiss-based constitutive relationship in a two-fluid system of equations. For the dust phase, computational models were developed based on the kinetic theory of the granular flows. Due to the orthogonal property of the basis functions in the method, no specific treatment of the source terms, commonly necessary in the conventional finite volume method, was required. Moreover, a high-fidelity approach was selected to treat the non-strictly hyperbolic equations of a dusty gas. This allows the same inviscid numerical flux functions to be applied to both the gaseous Euler and solid pressureless-Euler system of equations. Further, we observed that, for the discretization of the viscous fluxes in multiphase cases, the local discontinuous Galerkin is superior to the first method by Bassi and Rebay. After a verification and validation study, the new computational model was used to simulate the impingement of an underexpanded jet on a dusty surface in a rarefied condition. A surface erosion model based on viscous erosion associated with aerodynamic entrainment was implemented at a solid surface. Simulation cases in the near-field of the nozzle flow were tested to evaluate the

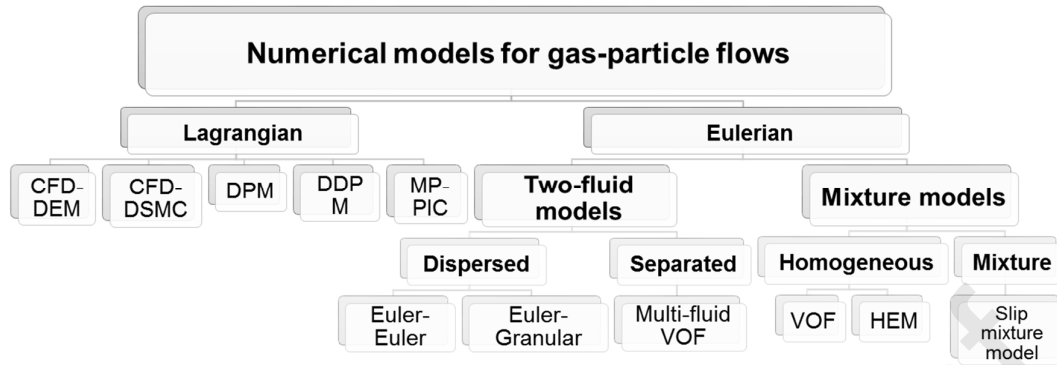
capabilities of the present computational model in handling the challenging problems of multi-scale multiphase flows.

Keywords: discontinuous Galerkin, two-fluid model, rarefied gases, granular flow

1. Introduction

Multiphase flows are observed in many geophysical flows and industrial applications. One significant class of multiphase flows is the gas-solid flow, which involves a flow of gases (carrier phase) with suspended rigid particles (particulate phase). Some technological examples include the transport of nanoscale soot particulates in gas turbine engines, air-droplet mixed flow in atmospheric icing, explosions in coal mines, the separation of particulate matter from fluids, and the interaction of a rocket plume with lunar dust. Volcanic eruptions, cosmic explosions, and star formation are other natural geophysical examples. The gas-solid flow is considered to be a *dusty gas flow* when the interaction between the gas and particles is more dominant than particle-particle interactions. The gas-solid flow is considered a *granular flow* when the particle-particle or wall-particle interactions are more dominant compared to the interstitial forces. And when the gas passes through a porous solid structure with pores—sometimes as small as the mean free path of the gas molecules—the gas-solid flow is called a *gas flow in porous media*.

The categories of mathematical models used to describe dusty gas flows (generalizable to other multiphase classes) are illustrated in **Table 1**. In the Lagrangian framework (alternatively known as the *trajectory*, *non-continuum* or *Eulerian-Lagrangian* model), each particle is tracked through space based on Newton's equation of motions. In the Eulerian framework (also known as the *continuum* or *Eulerian-Eulerian* model), the particles are considered a continuum, and a set of partial differential equations in a given coordinate system is derived to characterize the flow. A third category (or a sub-category of the *Eulerian models*) is called the *mixture* models, where both phases are defined by solving the continuum-based equation of a single fluid with modified properties.

Table 1. Mathematical models for simulating particulate flows.

In the present study, the two-fluid model is chosen over the trajectory model, since it is not only applicable to a broad spectrum of particulate loading in multi-phase regimes but also has less computational cost, compared with the Lagrangian counterpart. The model is, however, not efficient when the distribution in particle size is the primary interest, since a separate set of equations must be solved for each diameter size. The *pressureless* Euler equations, when applied as the mathematical model to describe the solid phase, have been shown to provide reasonable predictions in a variety of multi-phase/multi-fluid problems. Some examples include one-dimensional [1-5] and multi-dimensional [7-10] problems. It should be noted that, since the collision term scales with the square of the volume fraction of particles, the pressure and stress tensors of the solid-phase tend to vanish in the dilute limit, which makes the pressureless gas assumption valid in that regime.

However, when the role of particle-particle collisions is not negligible in the description of the solid phase, the closure for the stress tensor in the solid phase plays a significant role in mathematical modeling. The closure models are the main factor that distinguishes the various two-fluid models [11].

There are three approaches that are used to define the stress tensor in the solid phase (solid viscosity, more accurately). In the early models [12-14], experiments were used to describe the dependence of solid phase pressure on the particle volume fraction, and thus, an empirical constant was used to define the solid viscosity. These models are known as *constant viscosity models* (CVM).

The other class of models, by using the analogy from the gas phase, defines the viscosity. These models are, however, restricted to dilute dusty gas flows since the effect of particle-particle collisions is not included. On the other hand, efforts based on the kinetic theory, which adopt an analogy similar to rarefied gas flows, have led to the so-called *kinetic theory*

of granular flows (KTGF), which is a class of closure models for kinetic-collisional stresses [15-19]. This type of approach provides a link between the microscopic and macroscopic descriptions of the granular flow. Even though these models have mainly been applied to simulate fluidized beds and moving beds in the majority of previous works, with a reasonable level of approximation, they can be used in other applications where modeling particle-particle interactions (through binary and frictional contacts) is crucial [18, 20, 21].

One must keep in mind that the granular flow of particles is significantly different from molecular gas flows. The main differences are 1) elastic and inelastic collisions occur in gases while elastic-plastic deformation and surface friction occur in particles and, 2) kinetic energy is conserved in an isothermal system for gases while an equilibrium state does not exist in granular systems without external energy sources [11]. Schneiderbauer *et al.* [19] demonstrated that this class of models could provide substantial improvement compared with simulations using the discrete element method (DEM). Two-fluid models based on KTGF have shown a desirable capability by providing particle pressure, viscosity, and other transport coefficients; besides, less *ad hoc* adjustments are required, compared with the aforementioned models. The KTGF models are also known to provide promising results when the volume fraction of particles is less than 40% (where the assumption of binary collisions holds). When the solid volume fraction is higher, the solid phase undergoes multiple particle-particle frictional contacts, and the kinetic theory then fails to explain the physics of dense granular media.

The Eulerian models based on *mono-kinetic closure models*, even though they are capable of correctly predicting the formation of depletion zones and stiff accumulation regions, have difficulty in describing the so-called *particle trajectory crossing* (PTC) for high Stokes number flow. This limitation has motivated the introduction of a class of method of moments that allows for the coexistence of several velocities at the same location by solving higher order moments and applying Gaussian closures [10, 22-24]. On the other hand, using an approach based on the integral solution of the kinetic model in the flux evaluation across the cell interface, Liu *et al.* [25] proposed a scheme for dilute disperse gas-particle multiphase flows (UGKS-M) in a finite volume framework. Promising results were demonstrated, which could satisfactorily resolve the PTC and wall reflecting phenomena.

In most of the aforementioned studies, the main focus has been on the correct modeling of the dust phase, and for the gas phase, either classical Euler or Navier-Stokes-Fourier (NSF)

equations were solved, depending on the physics considered. However, in flows far from thermal equilibrium, these traditional models cannot predict the flow accurately. A case in point is the impingement of a rocket plume on the lunar surface, and the subsequent dusty gas flows formed by the ejection of solid particles from the regolith during the descent phase of the lunar lander [26]. These dusty gas flows are directly related to the number one concern in returning to the Moon claimed by the Apollo astronaut John Young [27]. The coexistence of various flow physics, such as the transition from continuum to rarefied flow condition, stand-off shock waves, stagnation regions, viscous boundary layers, the transition from subsonic to supersonic flow, surface erosion and particle entrainment in the rarefied condition, makes the computational simulation of the flow problem a very challenging topic.

Other examples that require the application of high-order models beyond the linear first-order NSF in a gas-solid multiphase flow are the study of the effect of micro-dust on heat transfer characteristics in micro/nano-channels, such as computer chip-sets or hard disk drives. Another important topic is the simulation of supersonic impactors (also known as pressure impactors) used in the classification of nanoparticles. The working principle of supersonic impactors is based on rarefaction effects [28].

A class of discretization methods that are gaining popularity from fluid mechanics problems to wave-related problems of acoustics and electromagnetics are the so-called high order—higher than second-order—spectral methods. The primary goal here is to provide a high-order conservative scheme that has a compact formulation and can handle complex geometries in a computationally efficient manner. In these methods, high order solution is achieved by increasing the polynomial order, and some of the popular subcategories include spectral difference (SD), spectral volume (SV), and flux reconstruction/correction procedure via reconstruction (FR/CPR) and discontinuous Galerkin (DG) method.

In the discontinuous Galerkin formulation, in contrast to its continuous counterpart, discontinuous basis functions are applied. This difference yields a local elemental mass matrix of the finite element formulation, instead of the globally coupled mass matrix of the continuous finite element method, making the DG method more flexible. For example, arbitrary triangulation with hanging nodes can be allowed. The p -adaptivity can be achieved by varying the polynomial degree, or the basis functions can even be defined for individual elements, independently of neighbor elements. Very high parallel efficiency is also

achievable because of its local data structure [29]. The DG method is called either modal [30-33] or nodal [34-37], depending on the type of basis functions.

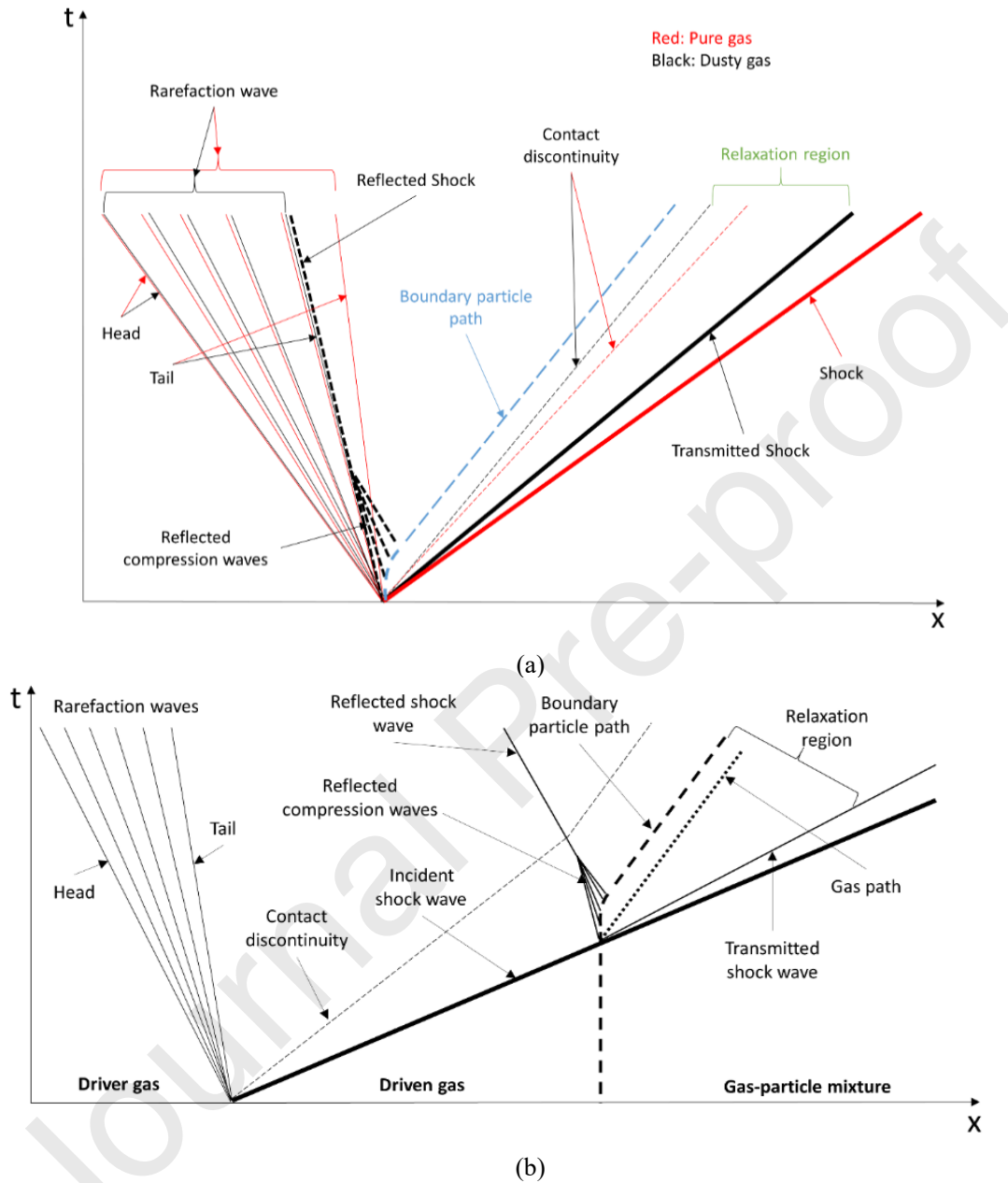


Fig. 1. Schematic of various wave structures in the 1-D dusty gas flows: (a) The gas contact discontinuity and boundary particle path are initially located at the same position, (b) The particle boundary path is located at a distance from the gas phase contact discontinuity. Reproduced with permission from O. Ejtehad, A. Rahimi, A. Karchani, R.S. Myong, “Complex wave patterns in dilute gas–particle flows based on a novel discontinuous Galerkin scheme,” *Int. J. Multiphase Flow* 104, 125 (2018). Copyright 2018 Elsevier.

While the DG method has been successfully applied to various classes of problems such as compressible and incompressible flows, aeroacoustics, magneto-hydrodynamics, and many

more [38], it has recently found its way into multiphase flow problems [39-45]. This is driven by recent advances in computational methods and computer resources, which make the DG method a feasible tool for more complicated applications.

The purpose of this work is to develop a modal discontinuous Galerkin method which can be applied to the two-fluid system of equations in the Eulerian framework and a broad spectrum of gas-phase regimes (from continuum to non-equilibrium) and solid-phase regimes (from dusty to granular gas flows). As a first step, an explicit modal DG scheme on triangular meshes was developed for solving multi-dimensional conservation laws of gas flows. That method was tested for simulations of all flow regimes of hypersonic rarefied and low-speed microscale gases [46-49] as well as dusty-gas flows [50, 51]. For dusty-gas flows [50], the zeroth-order Boltzmann-based constitutive relationships (Euler equations for the gas phase and pressureless Euler equations for the solid phase) were used to provide detailed discussions on the formation of intricate wave patterns, as depicted in **Fig. 1**. It should be noticed that complex wave patterns (i.e., pseudo-compound waves as well as composite waves) may occur in problems where moving shocks interact with a dusty medium.

In this study, by extending our previous work [50], we develop a modal discontinuous Galerkin method which can handle a far broader spectrum of gas-phase regimes (from continuum to non-equilibrium) and solid-phase regimes (from dusty to granular gas flows) in a unified framework. The non-equilibrium effects in the gas phase are taken into account by using the second-order Boltzmann-Curtiss-based model based on Eu's cumulant expansion and Myong's closing-last balanced closure [52-54], which has shown high potential in the prediction of rarefied and microscale gas flows [46-49, 54, 55]. Moreover, the critical particle-particle interactions in granular gas flows are described based on the KTGF models as constitutive relations for the solid phase.

2. Background

There is growing interest in planetary explorations to the Moon, Mars, comets and asteroids, and various space missions are being planned by major space organizations, for example, NASA, ESA, JAXA, CNSA, and ISRO. Certain findings gained during the Apollo missions are relevant to those future expeditions. They revealed, for example, that during the lunar landing, due to the interaction of the descent engine rocket plume and the dusty surface of the Moon, the surface could be substantially eroded, leading to dispersion of dust particles into the flow field. The astronauts who walked on the Moon reported that electrically charged

dust particles were one of the most challenging issues during the landing phase of the Apollo lunar missions [56]. Thus, understanding the physical nature of the interaction of the plume and dusty surface is a crucial step in the design phase of lunar/martian missions.

It is worth mentioning that creating an experimental setup in which a rocket engine is fired into a dusty bed—with many unknown characteristics—while maintaining the vacuum and low gravity conditions of the Moon is a daunting task, if not impossible. This fact makes theoretical studies and, in particular, computational fluid dynamics, an essential tool to study this kind of problem.

The most widely applied method of simulating rarefied multiphase flows is the direct simulation Monte Carlo (DSMC) method or hybrid CFD-DSMC methods [57-59], which have been proven to provide fairly accurate results for highly non-equilibrium flows. Since the DSMC method can be applied in a Lagrangian formulation, the dust phase can be handled with minor modifications to the general algorithm. However, the multiscale nature of the problem in which various Knudsen and Mach regimes coexist makes the application of the DSMC method computationally very expensive, and in particular, when simulating the whole transient phase of the flow.

Furthermore, the hybrid method may not be suitable for cases where particles are present in the continuum domain of a hybrid solver. For example, when simulating liquid hydrocarbon fuels, incomplete combustion due to insufficient mixing of oxidizer and fuel leads to carbon soot formation. The flow can be two-phase inside the nozzle, where the DSMC solvers are extremely inefficient due to characteristics of the flow (low Knudsen numbers). Another problematic condition for hybrid solvers is simulating flow very close to the Moon surface (before engine shut down) where the chances of finding eroded particles in the continuum region are high. In such cases, the hybrid methods must be modified so that the DSMC solver is active only in the continuum regime for the dust phase, which adds to the complexity of the implementation.

Few previous works have numerically investigated the interaction of plume impingement and solid particles due to either erosion or other sources (for example, soot formation in solid propellants rockets) in a rarefied condition. Burt and Boyd [60] extended the DSMC approach proposed by Gallis *et al.* [61] to simulate the transport of spherical particles in a rarefied gas flow in such a way that the two-way coupling effect was taken into account. In a similar work but with a different approach, Gimelshein *et al.* [62] developed a two-way

combined continuum-DSMC algorithm and applied the method to a two-phase plume flow produced by a side jet of a small-size aluminized propellant interacting with the rarefied freestream air flow.

Liu *et al.* [63] developed a numerical approach, adopting the DEM method to simulate a single dust particle ejection. The particles were then overlaid in the flow field obtained by the DSMC and gas kinetic Bhatnagar–Gross–Krook (BGK) method. However, because of the deterministic nature of the DEM method, this approach was found to be computationally very costly. He *et al.* [57] extended the DSMC method to incorporate molecule–molecule, molecule–particle, and particle–particle collisions and applied the method to the problem of lunar landing. Morris *et al.* [58, 64] developed a loosely coupled CFD/DSMC method in which the DPLR (NASA's continuum flow solver [65]) was used to calculate the nozzle core flow, while the DSMC method was applied to calculate the rarefied region and solid phase. Promising results were obtained, and the work was later extended to three-dimensional problems [59]. On the other hand, Rahimi *et al.* [66] recently computationally investigated the near-field interaction of the plume and surface in a low altitude hover on the order of a few meters using the first-order NSF constitutive relationships and the discrete phase model which handles the particulate phase in a Lagrangian framework.

A rough but sensible classification of the regimes and definitions of the three important regions in nozzle proximity are provided in **Fig. 2**. The particulate loading and the Stokes number can be used to characterize the flow. In region 1, just beneath the nozzle, the onset of erosion occurs. Here the gas flow after passing through the strong stand-off shock wave would stagnate because of a collision with the surface. In this region, the static pressure reaches a maximum, while the gas velocity remains minimum. In region 2, the fictitious passage formed by the stand-off shock and the surface acts as a converging-diverging passage accelerating the gas to reach supersonic velocities. The maximum erosion occurs at the surface in this region. In region 3, both the dust particles and gas molecules expand further into the near-vacuum condition and undergo free-molecular movement with high velocities. Previous simulation studies have indicated that the granular flows in the limits of suspensions and early fluidized bed may appear depending on the erosion rate.

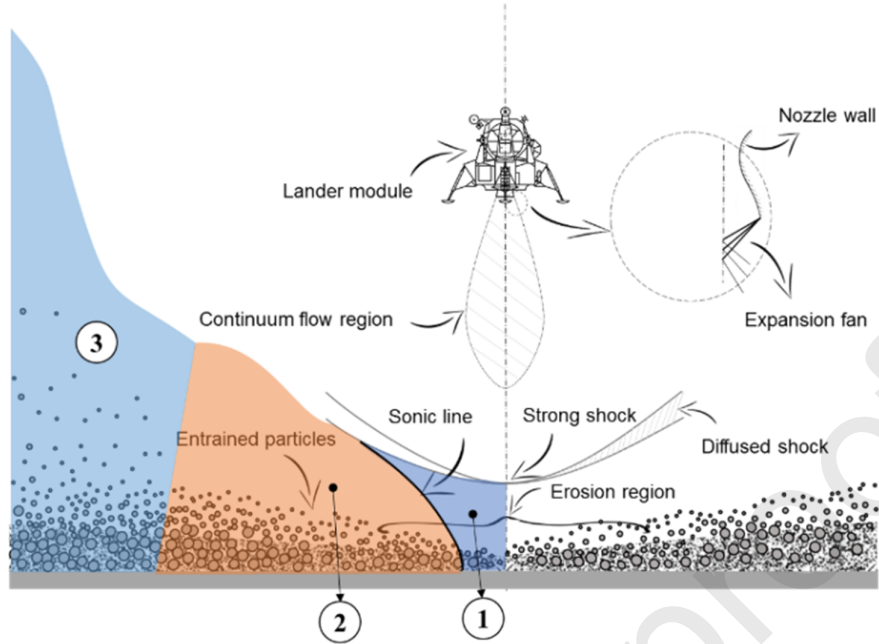


Fig. 2. Graphical categorization of different regions with various specifications in the problem of lunar landing.

Table 2. Range of important parameters in different regions present in lunar landing.

	Region 1	Region 2	Region 3
\mathbf{u}_g	Very low	High	High
\mathbf{u}_s	0	Low	High
ρ_g	$O(10^{-3})$	$O(10^{-4})$	$\geq O(10^{-4})$
ρ_s	Constant	Constant	Constant
α_s	Very low	High	Intermediate
α_g	≈ 1	Low	Intermediate
β	≈ 0	Intermediate	High
St	$\ll 1$	< 1	≈ 1

As can be seen in **Table 2**, various multiphase regimes coexist in the present flow problem, clearly indicating the need for a unified multiphase solver, which can cover a wide range of Knudsen and Mach regimes. For this purpose, a two-fluid model is employed to take the multiphase effects into account. The conservation laws are solved in conjunction with the

Boltzmann-based constitutive models for both phases. The proposed method can be used in other problems where dust particles (with a wide range of volume fractions) are present in a gas mixture in either continuum or non-equilibrium conditions.

3. Mathematical modeling of rarefied and multiphase flows in the Eulerian framework

In the lunar landing problem, a wide range of particulate loadings may exist. The Eulerian models can provide acceptable results in a wide range of applications—especially when the volume fraction of the two phases is comparable or when the interaction of the phases signifies the hydrodynamic feature of the flow. In **Fig. 3**, the flow regimes in the lunar landing problem are categorized based on the volume fraction of particles, number density, and particle diameter. The regime of interest can be determined based on the approximate values of the parameters for a lunar landing case like the Apollo lander, as marked in **Fig. 3**.

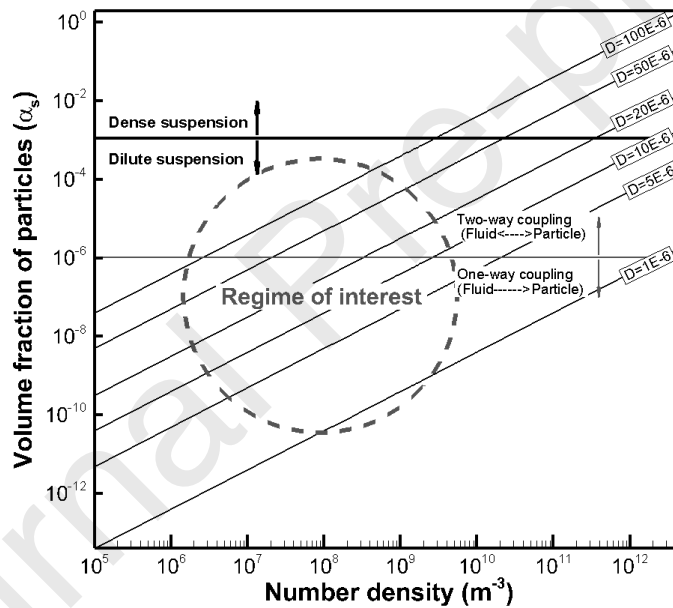


Fig. 3. Regimes encountered in the lunar landing problem overlaid on the classification of the particulate flows based on number density and particles volume fraction.

The regime of main interest falls in the category of the dilute suspension. With larger particle diameters, when the number densities or volume fractions are higher, the regime may belong to the category of dense suspensions, and thus further considerations need to be taken into account. In this work, to cover regimes encountered in the typical lunar landing problem, the two-fluid Eulerian model was employed as the most efficient approach, and applied for the test cases considered. In the lunar landing problem, predicting the shape and location of

the gas-solid interface is not essential, and thus dispersed Eulerian models can describe the main characteristics of the flow regimes.

3.1. Two-fluid model equations for dusty gas flows

In the majority of two-fluid *Euler-Euler* models for dusty gas flows, the gas phase is considered a compressible gas, which follows the perfect-gas law, while the solid phase respectively as incompressible [7, 67-69]. The inter-particle collisions are neglected (thus no pressure term in the conservation laws for the solid phase), and the particles are assumed to be uniformly sized spheres with a constant diameter, density, and temperature. The specific heat of the particle material is also assumed to be constant. Moreover, the particles are considered to be inert, and the thermal and Brownian motions of particles are neglected. Furthermore, the gravitational and buoyant forces, the turbulence effects, and the effect of particles' wakes are considered to be negligible.

On the other hand, in the *Euler-granular* models the solid pressure and viscous fluxes are retained for the solid phase to simulate granular flows. In these two-fluid models, the number density of the particles should be large enough to avoid violating the continuum assumption.

Under the aforementioned conditions, the conservation laws (taking viscous effects and solid pressure into account) can be written as follows: for the gas phase,

$$\partial_t \mathbf{U}_g + \nabla \cdot \mathbf{F}_g = \mathbf{S}, \quad (1)$$

$$\mathbf{U}_g = \begin{bmatrix} \alpha_g \rho_g \\ \alpha_g \rho_g \mathbf{u}_g \\ \alpha_g \rho_g E_g \end{bmatrix}, \quad \mathbf{F}_g = \begin{bmatrix} \alpha_g \rho_g \mathbf{u}_g \\ \alpha_g \rho_g \mathbf{u}_g \mathbf{u}_g + p_g \mathbf{I} + \mathbf{\Pi}_g \\ (\alpha_g \rho_g E_g + p_g) \mathbf{u}_g + \mathbf{\Pi}_g \cdot \mathbf{u}_g + \mathbf{Q}_g \end{bmatrix}, \quad (2)$$

$$\mathbf{S}_g = \begin{bmatrix} 0 \\ D_{g,s} (\mathbf{u}_s - \mathbf{u}_g) \\ D_{g,s} (\mathbf{u}_s - \mathbf{u}_g) \mathbf{u}_s + Q_{g,s} (T_s - T_g) \end{bmatrix},$$

$$E_g = c_v T_g + \frac{1}{2} |\mathbf{u}_g|^2, \quad (3)$$

and, for the solid phase,

$$\partial_t \mathbf{U}_s + \nabla \cdot \mathbf{F}_s = -\mathbf{S}, \quad (4)$$

$$\mathbf{U}_s = \begin{bmatrix} \alpha_s \rho_s \\ \alpha_s \rho_s \mathbf{u}_s \\ \alpha_s \rho_s E_s \\ \alpha_s \rho_s e_s \end{bmatrix}, \quad \mathbf{F}_s = \begin{bmatrix} \alpha_s \rho_s \mathbf{u}_s \\ \alpha_s \rho_s \mathbf{u}_s \mathbf{u}_s + p_s \mathbf{I} + \mathbf{\Pi}_s \\ (\alpha_s \rho_s E_s + p_s) \mathbf{u}_s + \mathbf{\Pi}_s \cdot \mathbf{u}_s + \mathbf{Q}_s \\ \alpha_s \rho_s e_s \mathbf{u}_s \end{bmatrix}, \quad (5)$$

$$\mathbf{S}_s = \begin{bmatrix} 0 \\ D_{g,s}(\mathbf{u}_s - \mathbf{u}_g) \\ D_{g,s}(\mathbf{u}_s - \mathbf{u}_g) \mathbf{u}_s + Q_{g,s}(T_s - T_g) \\ \dot{\gamma} \end{bmatrix},$$

$$E_s = c_m T_p + \frac{1}{2} |\mathbf{u}_s|^2, \quad (6)$$

$$e_s = \frac{3}{2} \Theta, \quad (7)$$

$$\alpha_g + \alpha_s = 1. \quad (8)$$

Here the \mathbf{U} , \mathbf{F} , and \mathbf{S} are the vectors of the conservative variables, fluxes, and source terms, respectively. The variables t , α , ρ , \mathbf{u} , E , p , T , $\mathbf{\Pi}$, and \mathbf{Q} represent time, volume fraction, density, velocity vector, total energy, pressure, temperature, viscous stress tensor, and heat flux vector. In equation (5), $\dot{\gamma}$ is the dissipation of pseudo-thermal energy (PTE) due to inelastic particle collisions. Further, D and Q represent the interphase drag and heat flux, respectively. In the Euler-granular model, a new equation for PTE e_s is solved to yield the granular temperature Θ . The dust density ρ_s is assumed to be constant; thus, solid-phase compressibility is controlled by the changes in the solid volume fraction.

3.2. Second-order Boltzmann-Curtiss-based hydrodynamics model for modeling gas in thermal non-equilibrium using method of moments

3.2.1. Conservation laws from the Boltzmann-Curtiss kinetic equation

Because of the collisional invariant properties of mass, momentum, and energy, the exact conservation laws can be derived from the Boltzmann-Curtiss kinetic transport equation. The Boltzmann-Curtiss kinetic equation for diatomic (and linear polyatomic) molecules with a moment of inertia I_m and an angular momentum \mathbf{j} can be expressed [70] as follows,

$$\left(\frac{\partial}{\partial t} + \mathbf{v} \cdot \nabla + \frac{\mathbf{j}}{I_m} \frac{\partial}{\partial \psi} + F \cdot \nabla_v \right) f(\mathbf{v}, \mathbf{r}, \mathbf{j}, \psi, t) = C[f, f_2], \quad (9)$$

where $f, \mathbf{v}, \mathbf{r}, \psi, j$ and $C[f, f_2]$ represent the distribution function, the particle velocity, the particle position, the azimuthal angle associated with the orientation of the particle, the magnitude of the angular momentum vector \mathbf{j} , and the collision integral, respectively. F is the external force on unit mass, and ∇_v denotes the gradient vector in the velocity space. The Boltzmann-Curtiss kinetic equation describes the changes in the probability distribution function along a molecular pathway due to intermolecular collisions and under the presence of external force F .

The conservation laws of mass, momentum, and total energy for monatomic gases can be derived directly from the Boltzmann-Curtiss kinetic equation by noting that the molecular expressions for conserved variables are collision invariants. After differentiating the statistical definition of the conserved variables with time and combining them with the Boltzmann-Curtiss kinetic equation, the following conservation laws, all of which are an exact consequence of the Boltzmann-Curtiss kinetic equation, can be derived [52, 71, 72]: in the absence of external force,

$$\frac{\partial}{\partial t} \begin{bmatrix} \rho \\ \rho \mathbf{u} \\ \rho E \end{bmatrix} + \nabla \cdot \begin{bmatrix} \rho \mathbf{u} \\ \rho \mathbf{u} \mathbf{u} + p \mathbf{I} \\ (\rho E + p) \mathbf{u} \end{bmatrix} + \nabla \cdot \begin{bmatrix} 0 \\ \mathbf{\Pi} + \Delta \mathbf{I} \\ (\mathbf{\Pi} + \Delta \mathbf{I}) \cdot \mathbf{u} + \mathbf{Q} \end{bmatrix} = 0. \quad (10)$$

There are two different sets of macroscopic variables; the conserved variables $(\rho, \rho \mathbf{u}, \rho E)$ and the non-conserved variables $(\mathbf{\Pi}, \Delta, \mathbf{Q})$, where \mathbf{u} is the bulk velocity vector, E is the total energy density, while $\mathbf{\Pi}, \Delta, \mathbf{Q}$ represent the shear stress tensor, the excess normal stress, and the heat flux, respectively. It should be noted that the set of equations (10) remain open unless non-conserved variables are determined. Because of the presence of the non-conserved variables $\mathbf{\Pi}, \Delta, \mathbf{Q}$ (whose molecular definitions do not yield a collisional invariant), the evolution equations of these variables should be derived.

3.2.2. Boltzmann-Curtiss-based constitutive relationships for the gas phase

The exact same approach used to derive the conservation laws can be applied to the derivation of the evolution equation of non-conserved variables. After differentiating the statistical definition of the corresponding non-conserved variables with time and combining them with the Boltzmann-Curtiss kinetic equation, the following first-order Boltzmann-Curtiss-based constitutive model of the shear stress tensor, the excess normal stress, and heat flux vector can be derived:

$$\begin{aligned}
 \mathbf{\Pi}_g &= -2\mu_g [\nabla \mathbf{u}_g]^{(2)}, \\
 \Delta_g &= -\mu_b \nabla \cdot \mathbf{u}_g, \\
 \mathbf{Q}_g &= -\kappa_g \nabla T_g.
 \end{aligned} \tag{11}$$

The symbol $[\mathbf{A}]^{(2)}$ denotes the traceless symmetric part of the second-rank tensor \mathbf{A} . It should be mentioned that these first-order linear relations were obtained after very crude first-order approximations; all kinematic terms except for the thermodynamic force term were neglected in the evolution equations and the collision-related dissipation terms were linearized. Moreover, a distinction should be made regarding Navier-Fourier (NF) and Navier-Stokes-Fourier (NSF) relations. In the latter, the Stokes' hypothesis, $\mu_b = 0$, was applied.

Similarly, the second-order Boltzmann-Curtiss-based constitutive models can be derived by first differentiating the statistical definition of the non-conserved variables with time and then combining them with the Boltzmann-Curtiss kinetic equation. Once the two tenets—Eu's cumulant expansion based on the canonical distribution function in the exponential form to the explicit calculation of the dissipation term [73, 74], and Myong's closing-last balanced closure [72]—are applied to the evolution equations and after introducing the so-called adiabatic approximation derived from the observation that the relaxation times of the non-conserved variables are very short, being on the order of 10^{-10} second, the following second-order constitutive model can be derived from the Boltzmann-Curtiss kinetic equation [52, 71, 72]:

$$\begin{aligned}
 \hat{\mathbf{\Pi}} q_{2nd}(c\hat{R}) &= (1 + f_b \hat{\Delta}) \hat{\mathbf{\Pi}}_0 + [\hat{\mathbf{\Pi}} \cdot \nabla \hat{\mathbf{u}}]^{(2)} \\
 \hat{\Delta} q_{2nd}(c\hat{R}) &= \hat{\Delta}_0 + \frac{3}{2} f_b (\hat{\mathbf{\Pi}} + f_b \hat{\Delta} \mathbf{I}) : \nabla \hat{\mathbf{u}} \\
 \hat{\mathbf{Q}} q_{2nd}(c\hat{R}) &= (1 + f_b \hat{\Delta}) \hat{\mathbf{Q}}_0 + \hat{\mathbf{\Pi}} \cdot \hat{\mathbf{Q}}_0 \\
 \text{where } q_{2nd}(c\hat{R}) &= \frac{\sinh(c\hat{R})}{c\hat{R}}, \quad \hat{R}^2 \equiv \hat{\mathbf{\Pi}} : \hat{\mathbf{\Pi}} + \frac{(5-3\gamma)}{f_b} \hat{\Delta}^2 + \hat{\mathbf{Q}} \cdot \hat{\mathbf{Q}}.
 \end{aligned} \tag{12}$$

The caret (^) over a symbol represents a quantity with the dimension of the ratio of the stress to the pressure. The values of $\mathbf{\Pi}_0$, Δ_0 , and \mathbf{Q}_0 are determined by the Newtonian law of shear and bulk viscosity and the Fourier law of heat conduction, respectively. \hat{R} represents the Rayleigh-Onsager dissipation function [75], and the constant c has a value between 1.0138 (Maxwellian) and 1.2232; for instance, 1.018 for the nitrogen gas molecule [52, 71, 72]. The

factor $f_b = \mu_b/\mu$ is the ratio of the bulk viscosity to the shear viscosity. Its value may be experimentally determined using a sound wave absorption measurement; for instance, 0.8 for the nitrogen gas molecule. Even though the second-order constitutive model (12) involves highly nonlinear implicit algebraic equations, they can be easily solved numerically for the given thermodynamic driving forces, based on the concept of decomposition and the method of iteration [52, 71, 72]. More details regarding the second-order Boltzmann-based and Boltzmann-Curtiss-based constitutive relationships and the closing-last balanced closure can be found in [52-54, 72].

3.3. Constitutive relationships for the solid phase

In generic KTGF models, to achieve explicit expressions for the non-conserved variables, the distribution function is expanded from the equilibrium distribution function via the Chapman-Enskog expansion to yield the following expansion

$$\mathbf{P}_s = p_s \mathbf{I} + \mathbf{\Pi}_s, \quad (13)$$

$$\mathbf{Q}_s = -\kappa_s \nabla T_s, \quad (14)$$

where

$$\mathbf{\Pi}_s = -\mu_s \left[(\nabla \mathbf{u}_s) + (\nabla \mathbf{u}_s)^T \right] - \left(\lambda_s - \frac{2}{3} \mu_s \right) [(\nabla \cdot \mathbf{u}_s) \mathbf{I}]. \quad (15)$$

The pressure p_s and the coefficients in the above relations, viz., κ_s , μ_s , λ_s , can be determined if the collision integrals of the Boltzmann-type kinetic equation for the solid particles are known. A simple linear BGK model will not provide desirable results for the solid phase since it does not contain a description of particle-particle interactions. Thus, after introducing a joint probability function $f_s^{(2)}$ in terms of solid distribution function f_s and pair distribution function g (which itself is dependent upon the distance $r_{12} = |\mathbf{r}_2 - \mathbf{r}_1|$ and the solid fraction) [11], explicit expressions can be derived for pressure, shear viscosity, and thermal conductivity by computing the collision integral of the solid phase,

$$p_s = \alpha_s \rho_s T_s, \quad (16)$$

$$\mu_s = \frac{5}{96} \pi \rho_s d \sqrt{\frac{T_s}{\pi}}, \quad (17)$$

$$\kappa_s = \frac{75}{384} \pi \rho_s d \sqrt{\frac{T_s}{\pi}}. \quad (18)$$

The above expressions are derived for sufficiently low particle density (where $g=1$) and can thus be applied to the limit of dilute flow. According to Chapman and Cowling [76], the shear viscosity and thermal conductivity of standard Enskog theory (SET) can be defined as

$$\mu_s^{SET} = c_1 \mu_s \left(\frac{1}{\chi b \rho_s} + \frac{4}{5} + \frac{4}{25} \left(1 + \frac{12}{\pi c_2} \right) \chi b \rho_s \right) b \rho_s, \quad (19)$$

$$\kappa_s^{SET} = c_1 \kappa_s \left(\frac{1}{\chi b \rho_s} + \frac{4}{5} + \frac{4}{25} \left(1 + \frac{12}{\pi c_2} \right) \chi b \rho_s \right) b \rho_s, \quad (20)$$

where $\chi = g(\alpha_s) = \left[1 - (\alpha_s / \alpha_{s,max})^{1/3} \right]^{-1}$ and $b = 2\alpha_s \pi d^3 / 3m$. Taking $c_1=c_2=1.0016$, the relations (19) and (20) can be reduced to,

$$\mu_s^{SET} = \mu_s \left(\frac{1}{\chi b \rho_s} + \frac{4}{5} + 0.7614 \chi b \rho_s \right) b \rho_s, \quad (21)$$

$$\kappa_s^{SET} = \kappa_s \left(\frac{1}{\chi b \rho_s} + \frac{4}{5} + 0.7614 \chi b \rho_s \right) b \rho_s. \quad (22)$$

The coefficient 0.7614 is slightly different from the coefficient 0.771 in most expressions in the literature including [17] with $c_1=c_2=1$. Moreover, the pressure of a dense system is given by [77] as follows,

$$p_s^{SET} = p_s (1 + y^{SET}), \quad (23)$$

where y^{SET} is the excess compressibility of the elastic hard-sphere system given by

$$y^{SET} = \chi b \rho_s = 4\chi \alpha_s. \quad (24)$$

The generic form of y^{SET} can be written as a function of α_s

$$y^{SET}(\alpha_s) = \frac{\sum_{n=0} c_n (4\alpha_s)^{n+1}}{\left(1 - (\alpha_s / \alpha_{cp})^a\right)^b}. \quad (25)$$

A comparison of y^{SET} values in the above relation used in references [78-80] with MD simulations [81, 82] was provided in reference [11].

4. A modal positivity/monotonicity preserving discontinuous Galerkin method

To solve the system of equations of the conservation laws, the modal discontinuous Galerkin method was selected. The DG method combines key features of the finite element and finite volume methods. The DG method was first introduced by Reed and Hill [83] and was extensively developed in [31, 84, 85]. Recently, the DG method has become a prominent tool for solving the fluid dynamics equations in different fields, including compressible and incompressible flows, aeroacoustics, magneto-hydrodynamics, multiphase flows, and many more [38].

4.1 A modal discontinuous Galerkin method for rarefied dusty gas flows

The mathematical model of interest in the present work can be written in a compact form;

$$\partial_t \mathbf{U} + \nabla \cdot \mathbf{F}_{inv}(\mathbf{U}) + \nabla \cdot \mathbf{F}_{vis}(\mathbf{U}, \nabla \mathbf{U}) = \mathbf{S}(\mathbf{U}) \quad \text{in } \left[(t, \Omega) \mid t \in (0, \infty), \Omega \subset \mathbb{R} \right], \quad (26)$$

where Ω denotes a bounded domain, and \mathbf{U} , \mathbf{F}_{inv} , \mathbf{F}_{vis} , \mathbf{S} represent conservative variables, inviscid flux, viscous flux, and source terms, respectively. The solution domain can be decomposed using a group of non-overlapping elements, $\Omega = \Omega_1 \cup \Omega_2 \cup \dots \cup \Omega_{ne}$, in which ne is the number of elements. By multiplying a weighting function φ_i into the conservative laws (26) and integrating over the control volume for each element, the following formulation can be derived:

$$\int_{\Omega_k} \left[\partial_t \mathbf{U} \varphi(\mathbf{x}) + \nabla \cdot \mathbf{F}_{inv}(\mathbf{U}) \varphi(\mathbf{x}) + \nabla \cdot \mathbf{F}_{vis}(\mathbf{U}, \nabla \mathbf{U}) \varphi(\mathbf{x}) - \mathbf{S}(\mathbf{U}) \varphi(\mathbf{x}) \right] d\Omega = 0. \quad (27)$$

As can be seen in (26) and (27), when the solution of viscous flows is the main interest, the derivatives of the conserved variable appearing in the viscous flux terms should be computed. These terms cannot be accommodated directly in a weak variational formulation using a discontinuous space function. One possible approach for circumventing the complexity is the addition of a set of separate equations to represent the gradient of the conservative variables as an auxiliary set of unknowns, as proposed by Bassi and Rebay [30].

In this work, the auxiliary variable \mathbf{A} is chosen to be the derivatives of the conserved variables \mathbf{U} , i.e., $\mathbf{A} = \nabla \mathbf{U}$. This approach is known as the mixed DG formulation and results in the following coupled system:

$$\begin{aligned} \mathbf{A} - \nabla \mathbf{U} &= 0, \\ \partial_t \mathbf{U} + \nabla \cdot \mathbf{F}_{\text{inv}}(\mathbf{U}) + \nabla \cdot \mathbf{F}_{\text{vis}}(\mathbf{U}, \mathbf{A}) &= \mathbf{S}(\mathbf{U}). \end{aligned} \quad (28)$$

Then the solution of the primary and auxiliary variables can be approximated as,

$$\mathbf{U}_h = \sum_i^P U_i(t) \varphi_i(\mathbf{x}) \quad \text{and} \quad \mathbf{A}_h = \sum_i^P A_i(t) \varphi_i(\mathbf{x}). \quad (29)$$

where $U_i(t)$ and $A_i(t)$ denote the local degree of freedom for the primary and auxiliary variables, respectively. By multiplying a weighting function φ_i into the conservative laws and integrating over the control volume for each element, the following formulation can be derived:

$$\int_{\Omega_k} [\mathbf{A} \varphi(\mathbf{x}) - \nabla \mathbf{U} \varphi(\mathbf{x})] d\Omega = 0, \quad (30)$$

$$\int_{\Omega_k} [\partial_t \mathbf{U} \varphi(\mathbf{x}) + \nabla \cdot \mathbf{F}_{\text{inv}}(\mathbf{U}) \varphi(\mathbf{x}) + \nabla \cdot \mathbf{F}_{\text{vis}}(\mathbf{U}, \mathbf{A}) \varphi(\mathbf{x}) - \mathbf{S}(\mathbf{U}) \varphi(\mathbf{x})] d\Omega = 0. \quad (31)$$

By splitting the integral over Ω_h into a series of integrals over the sub-elements and applying the integration by part as well as divergence theorem to the equations (30) and (31), we have

$$\int_{\Omega_k} \varphi_i(\mathbf{x}) \mathbf{A}_h d\Omega_k - \oint_{\partial\Omega_k} \varphi_i(\mathbf{x}) \mathbf{U}_h \cdot \hat{n} d\sigma + \int_{\Omega_k} \nabla \varphi_i(\mathbf{x}) \cdot \mathbf{U}_h d\Omega_k = 0, \quad (32)$$

$$\begin{aligned} \int_{\Omega_k} \partial_t \mathbf{U}_h \varphi_i(\mathbf{x}) d\Omega_k + \oint_{\partial\Omega_k} \varphi_i(\mathbf{x}) \mathbf{F}_{\text{inv}}(\mathbf{U}_h) \cdot \hat{n} d\sigma - \int_{\Omega_k} \nabla \varphi_i(\mathbf{x}) \cdot \mathbf{F}_{\text{inv}}(\mathbf{U}_h) d\Omega_k \\ + \oint_{\partial\Omega_k} \varphi_i(\mathbf{x}) \mathbf{F}_{\text{vis}}(\mathbf{U}_h, \mathbf{A}_h) \cdot \hat{n} d\sigma - \int_{\Omega_k} \nabla \varphi_i(\mathbf{x}) \cdot \mathbf{F}_{\text{vis}}(\mathbf{U}_h, \mathbf{A}_h) d\Omega_k = \int_{\Omega_k} \varphi_i(\mathbf{x}) \mathbf{S}(\mathbf{U}_h) d\Omega_k \end{aligned} \quad (33)$$

where \hat{n} is the outward normal vector of the element interface, and $\mathbf{U}_h, \mathbf{A}_h$ are the p -exact polynomial approximated solutions of the \mathbf{U}, \mathbf{A} , respectively, on the discretized domain of Ω_h .

In this work, the Dubiner polynomials [86] were selected as basis functions, while a collapsed coordinate transformation was used to transform the triangles in the physical domain to the standard square elements, Ω_e , in which the coordinates (a, b) are bound by constant limits:

$$\mathcal{D} = \{(a, b) \mid -1 \leq a, b \leq 1\}. \quad (34)$$

Another transformation was introduced to transform the triangle in the physical space into the computational space where the new local coordinates have independent bounds, as depicted in Fig. 4.

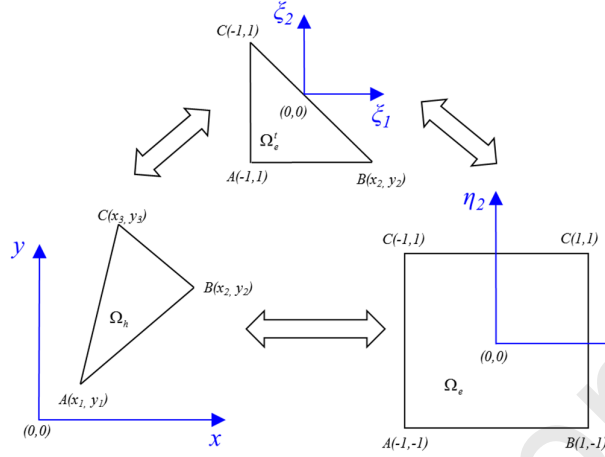


Fig. 4. Schematic diagram of the linear mappings of the 2D triangular element.

The process of estimating the surface and volume integrals is analogous to the inviscid system procedure detailed in [50]. However, for the auxiliary terms, more care should be paid to the details in the numerical implementation.

4.2 Implementation of numerical fluxes in multiphase cases

The choice of numerical flux can determine the stability and accuracy of the numerical method. In order to obtain a stable scheme, the numerical flux should be consistent as well as conservative. In our numerical code, the local Lax-Friedrichs (LLF) (or Rusanov [87]) and rotated-Harten-Lax-van Leer [88] fluxes, both of which are known to be simple and free from carbuncle phenomena, are implemented. Implementing the inviscid numerical flux is analogous to the well-established FVM procedure, and the details of the implementation can be omitted.

It should be noted that the AUSM family [89, 90] schemes have been widely used in many previous numerical works to simulate the dust phase. However, we aim to use the same flux scheme for both phases to be consistent. This may raise numerical difficulties when the solid pressure term in the model equations is not included. In this case, even though the system has real eigenvalues, they are not distinct; thus, the system becomes degenerate. Few approaches have been proposed to deal with this numerical issue in the past. Nevertheless, in the next

sub-section, a simple, easy to implement and yet effective method to circumvent this issue will be proposed.

The computation of the numerical viscous flux is not as straightforward in the DG framework as the inviscid flux. A rigorous mathematical derivation of the numerical flux functions for a pure elliptical Laplace equation can be found in [91, 92]. The unified analysis of the numerical schemes applied in this study, suggested by Arnold *et al.* [92] is summarized in **Table 3**. The operators $\{ \}$ and $\llbracket \rrbracket$ for scalar variable s and vector quantity \vec{v} are defined as follows,

$$\begin{aligned}\llbracket s \rrbracket &= s^+ \vec{n}^+ + s^- \vec{n}^- = \vec{n} (s^+ - s^-), \\ \{s\} &= \frac{1}{2} (s^+ + s^-), \\ \llbracket \vec{v} \rrbracket &= \vec{v}^+ \cdot \vec{n}^+ + \vec{v}^- \cdot \vec{n}^- = \vec{n} (\vec{v}^+ - \vec{v}^-), \\ \{\vec{v}\} &= \frac{1}{2} (\vec{v}^+ + \vec{v}^-).\end{aligned}\tag{35}$$

where the superscripts + and – indicate the left and right side of an element face.

Table 3. Comparison of the numerical schemes for viscous fluxes. \hat{u} and \hat{a} represent the numerical approximations to primary viscous and auxilliary flux values. Adapted from [92].

Method	\hat{u}	\hat{a}
Bassi and Rebay [30] (BR1)	$\{u_h\}$	$\{a_h\}$
Cockburn and Shu [93] (LDG)	$\{u_h\} - \beta \cdot [u_h]$	$\{a_h\} + \beta \llbracket a_h \rrbracket - \alpha_j (\llbracket u_h \rrbracket)$

The functional operators of α_i and α_j , the so-called penalty terms, are defined as

$$\begin{aligned}\alpha_j(\varphi) &= \mu \varphi = \eta_e h_e^{-1} \varphi, \\ \alpha_r(\varphi) &= -\eta_e \{r_e(\varphi)\},\end{aligned}\tag{36}$$

where η_e is a positive number, and h_e is an indicator of element size (e.g., the circumscribed circle radius of the element), and $\int_{\Omega} r_e(\varphi) \cdot \tau dx = - \int_e \varphi \cdot \{\tau\} ds$.

In this study, the BR1 and local discontinuous Galerkin (LDG) methods were implemented, depending on the problem. In the BR1 scheme, central discretization was used

for both the auxiliary and viscous fluxes. This method, which is extensively used by the DG community, is shown to have a convergence order of only P (polynomial degree) for odd ansatz [93]. Moreover, the stencil is known to not be compact. These deficiencies motivated the application of the LDG method, in which one-sided fluxes in opposite directions are used for both the auxiliary and viscous fluxes. In our simulations, β was set equal to zero when the LDG method was used. Our numerical experiments revealed that, when the Euler-granular (first-order constitutive equations for the dust phase) model was used, the use of the BR1 scheme made the numerical process unstable and led to instant divergence, while the LDG method quickly remedied the stability problem.

4.3. Circumventing the non-strict hyperbolicity of the dusty gas model equation

The non-strictly hyperbolic nature of the dusty gas model equation (related to the non-existence of a pressure term) can impose serious difficulties on numerical methods including the DG method. The issue can be circumvented either by considering the dispersed phase incompressible and adding a pressure term for numerical purposes [5, 94], or by considering both phases compressible. The former approach can yield a hyperbolic system but is not physically justifiable. On the other hand, the latter method can lead to unrealistic results in many two-phase flow problems [95].

In this study, a simple but very effective strategy is introduced to remedy this challenging issue. The idea was inspired by a strategy initially developed in computational magnetohydrodynamics (MHD) [96-98] which has since been applied in other fields, including aircraft icing in the atmosphere [99]. This is the first time this approach is being used for the two-fluid equation model of dusty gases.

The basic idea is to add and subtract a pressure-related term to the momentum and energy equations of the dust phase. Even though this manipulation does not have any mathematical consequences, from a numerical point of view, the new system has an obvious advantage, recovering the strict hyperbolicity of the equation. The equation for the dust phase (in the Euler-Euler model) after the addition and subtraction of a pressure-related term can be written as follows,

$$\partial_t \begin{bmatrix} \alpha_s \rho_s \\ \alpha_s \rho_s \mathbf{u}_s \\ \alpha_s \rho_s E_s \end{bmatrix} + \nabla \cdot \begin{bmatrix} \alpha_s \rho_s \mathbf{u}_s \\ \alpha_s \rho_s \mathbf{u}_s \mathbf{u}_s + p_s \mathbf{I} - p_s \mathbf{I} \\ (\alpha_s \rho_s E_s + p_s - p_s) \mathbf{u}_s \end{bmatrix} = -\mathbf{S}. \quad (37)$$

Equivalently in split form,

$$\partial_t \begin{bmatrix} \alpha_s \rho_s \\ \alpha_s \rho_s \mathbf{u}_s \\ \alpha_s \rho_s E_s \end{bmatrix} + \nabla \cdot \begin{bmatrix} \alpha_s \rho_s \mathbf{u}_s \\ \alpha_s \rho_s \mathbf{u}_s \mathbf{u}_s + p_s \mathbf{I} \\ (\alpha_s \rho_s E_s + p_s) \mathbf{u}_s \end{bmatrix} = \nabla \cdot \begin{bmatrix} 0 \\ p_s \mathbf{I} \\ p_s \mathbf{u}_s \end{bmatrix} - \mathbf{S} \quad (38)$$

In this equation, the inviscid flux is equivalent to that of the Euler equation of the gas phase. Thus, the conservation law can be considered strictly hyperbolic, and the additional term in the right-hand side can be handled in a way that is similar to how the source terms are treated.

4.4. Positivity preserving scheme

High order numerical schemes, including the DG scheme introduced in the previous section, often suffer from non-physical negative density or pressure. This leads to the ill-posedness of the system and numerical breakdowns as a consequence. On the other hand, for conservation laws with source terms which account for chemical reactions, gravity, or the interaction of phases in the present case, there is an increased possibility of encountering negative density or pressure during numerical simulation. Therefore, the application of positivity preserving schemes is necessary to prevent the numerical breakdown.

In the present work, a positivity preserving scheme developed for compressible Euler equations by Zhang and Shu [100] was employed to ensure the positivity of density and pressure, while maintaining higher-order accuracy. The general implementation of the scheme can be outlined as follows.

Limiting the higher-order coefficients for density was achieved first by computing the minimum value of the density amongst all quadrature points, ρ_{\min} . The coefficients for the density expansion were then modified as $\tilde{a}_i^p = \theta_i a_i^p$ with $\theta_i = \min\left[\frac{(a_0^p - \mathcal{E})}{(a_0^p - \rho_{\min})}, 1\right]$. In this expression, the i index accounts for all the bases, and the zero index represents the mean solution. Also, the value \mathcal{E} was determined by $\mathcal{E} = \min(10^{-13}, a_0^p, \bar{p})$ where \bar{p} denotes the mean element pressure.

For the modification of pressure, the following procedures were used. First, we set \mathbf{s} as

$$\mathbf{s} = (1-t)\bar{\mathbf{w}} + \beta\bar{\mathbf{q}}, \quad (39)$$

where $\bar{\mathbf{w}}$ and $\bar{\mathbf{q}}$ are the cell average and conservative variables, respectively. β can be calculated as follows

$$\beta = \begin{cases} 1 & \text{if } p(\mathbf{q}) \geq \varepsilon \\ \text{the solution of } p(\mathbf{s}) = \varepsilon, & \text{if } p(\mathbf{q}) < \varepsilon \end{cases} \quad (40)$$

Finally, the coefficients were modified by $\tilde{a}_i^p = \theta_2 a_i^p$ with $\theta_2 = \min(\beta, 1)$.

The application of this limiter was confirmed to provide stable schemes for unstructured triangular meshes with favorable results [32]. We report the first application of this type of limiter to the two-fluid model of dusty gas flows. Our numerical experiments for all the test cases show that the application of a positivity preserving limiter is essential to obtain converged solutions without compromising the accuracy of the solution.

4.5. Monotonicity preserving scheme

Numerical investigations using the present DG scheme further show that the mere application of the positivity preserving scheme is not enough to develop a stable scheme, especially in the presence of strong shock waves. The situation worsens when the multiphase system with source terms is solved. The present study employs the limiter Zhang and Shu [101] developed for one-dimensional cases, and the limiter Barth and Jespersen [102] initially devised for the finite volume framework. It is important to note that the TVD/MUSCL type scheme can degrade the order of accuracy in the smooth regions of the solution unless a pragmatic shock detection scheme is introduced.

According to Barth and Jespersen [102], the limiting procedure of slopes should be performed in a way that the solution at the integration points is confined to the range spanned by the neighboring solution averages. The limited solution can then be written as

$$U(\mathbf{x}, t) = a_0(t)\varphi_0(\mathbf{x}) + \lambda_{\min} \sum_{i>0}^p a_i \varphi_i(\mathbf{x}), \quad (41)$$

where $\lambda_{\min} = \min \max(\lambda_1, 0)$,

$$\lambda_1 = \begin{cases} \min(1, \frac{U_{\max} - U_i}{\Delta_2}), & \text{if } \Delta_2 > 0 \\ \max(1, \frac{U_{\min} - U_i}{\Delta_2}), & \text{if } \Delta_2 < 0 \\ 1, & \text{otherwise.} \end{cases} \quad (42)$$

Here $\Delta_2 = U_j(\mathbf{x}_i^*) - U_j$ and U_{\max} and U_{\min} are the maximum and minimum solution averages of the elements sharing edges, respectively.

5. Numerical experiments on the second-order Boltzmann-Curtiss continuum model of solid-gas multiphase flows

The solution of model equations for a pure gas in thermal non-equilibrium (i.e., the second-order Boltzmann-Curtiss-based constitutive relation) using a discontinuous Galerkin method has previously been verified and validated for several benchmark problems [46, 47]. The DG solutions for two-fluid models based on 1) the zeroth-order constitutive relation for both gas and solid phases [50] and 2) the first-order constitutive relation for gas phase but the zeroth-order constitutive relation for dust phase [51] have been verified as well.

In the following, the problem of interaction between a shock wave and a loose dust layer is investigated to verify the DG solution of the Euler-granular model (zeroth-order and second-order constitutive relations for the gas and solid phases, respectively). The presence of a shock wave and its interaction with a dust layer resembles to a large extent the ultimate problem of the current work, i.e., modeling and simulation of the lunar landing problem. After the numerical studies, the under-expanded jet and finally the impingement of a jet on a dusty surface are solved. All the simulations were conducted using a second-order scheme (first-order polynomials, P^1) in space and third-order in time.

5.1. Interaction of a shock wave with a loose dust layer

The problem of a shock wave interacting with a loose dust layer has practical importance in various industrial applications. However, in this work, the problem was selected with the goal of verifying the DG solution of the Euler-granular model. When a planar shock passes by a loosely packed dust layer, entrained particles form a dust cloud and the shock will be curved. A schematic of the problem of a shock wave interacting with a dust layer, and the geometrical setup and boundary conditions, are shown in **Fig. 5**.

As with previous studies on this problem [20, 103], the length (L) and height (H) of the computational domain, the horizontal location of the shock front (x_S), the left edge of the dust layer (x_{DL}), and the height of the dust layer (H_{DL}) were set to 6 cm, 50 cm, 1 cm, 2 cm, and 2 cm, respectively. A particle diameter of 3 μm was selected. The particle properties correspond to coal dust with a particle density of 1,470 kg/m^3 and a specific heat of 987 $\text{Jkg}^{-1}\text{K}^{-1}$. The gas phase was initialized with a condition corresponding to a Mach 1.6 shock

propagating into the air with a pressure of 101,325 Pa and a temperature of 288 K. The dust layer is initialized with a volume fraction of 0.004. The cost-effective LLF flux function and LDG scheme for inviscid and viscous fluxes, and activation of positivity and monotonicity limiters were shown to be the critical factors in the numerical experiments.

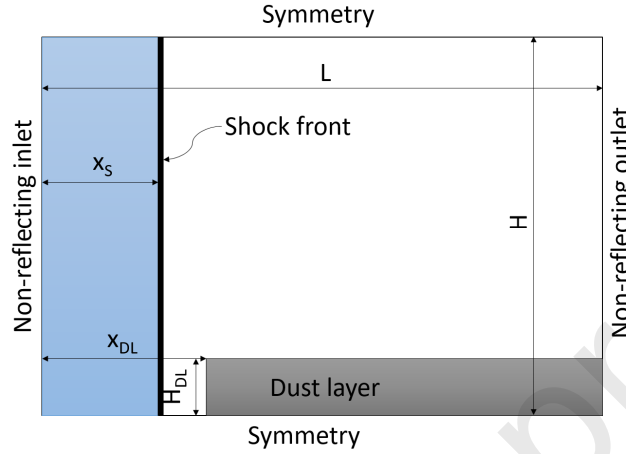


Fig. 5. Schematic of the problem of interaction of a shock wave with a dust layer.

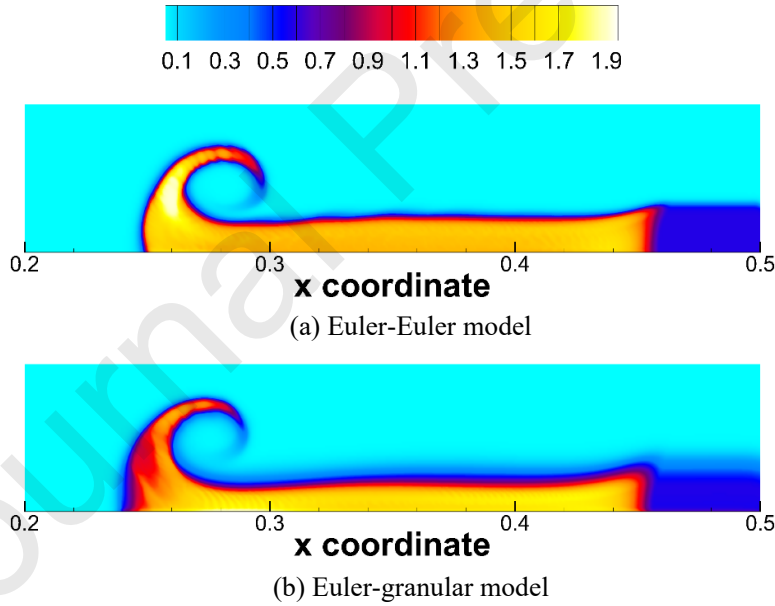


Fig. 6. A comparison of zeroth-order and second-order constitutive relations in the contours of concentration of solid phase: (a) Euler-Euler model, (b) Euler-granular model.

A comparison of the concentration of the solid phase computed by the zeroth-order (Euler-Euler) and the second-order (Euler-granular) constitutive relations is illustrated in **Fig. 6**. Contour plots of the instantaneous concentration show that both models predict an almost identical patterns in the general topology of the dust layer after interaction with the shock

wave. However, due to the viscous effect, the Euler-granular solution is more diffusive. Also, it can be seen that the dust layer is swept less and rises higher, compared with the Euler-Euler solution.

Fig. 7 depicts the effects of grid size and particle diameters. Three different grids with sizes of 1.2, 0.8, 0.4 mm were simulated to investigate how each grid resolved the rolling up of the dust pile caused by the gaseous drag. As can be seen in **Fig. 7** (a), the finer the grid, the more the rolling up of the dust particles is resolved. These grid sizes were chosen to be close to the values that were used by Houim and Oran [20]. Unlike previous studies which tackled this problem using either structured or quadrilateral grids, the present method used unstructured triangular grids that can more easily deal with complex arbitrary geometries. The contours of the concentration of the solid phase are plotted for three different particle diameters of 1, 5, and 10 μm in **Fig. 7** (b). The results show trends that are similar to the solutions of Fedorov and Kharlamova [103].

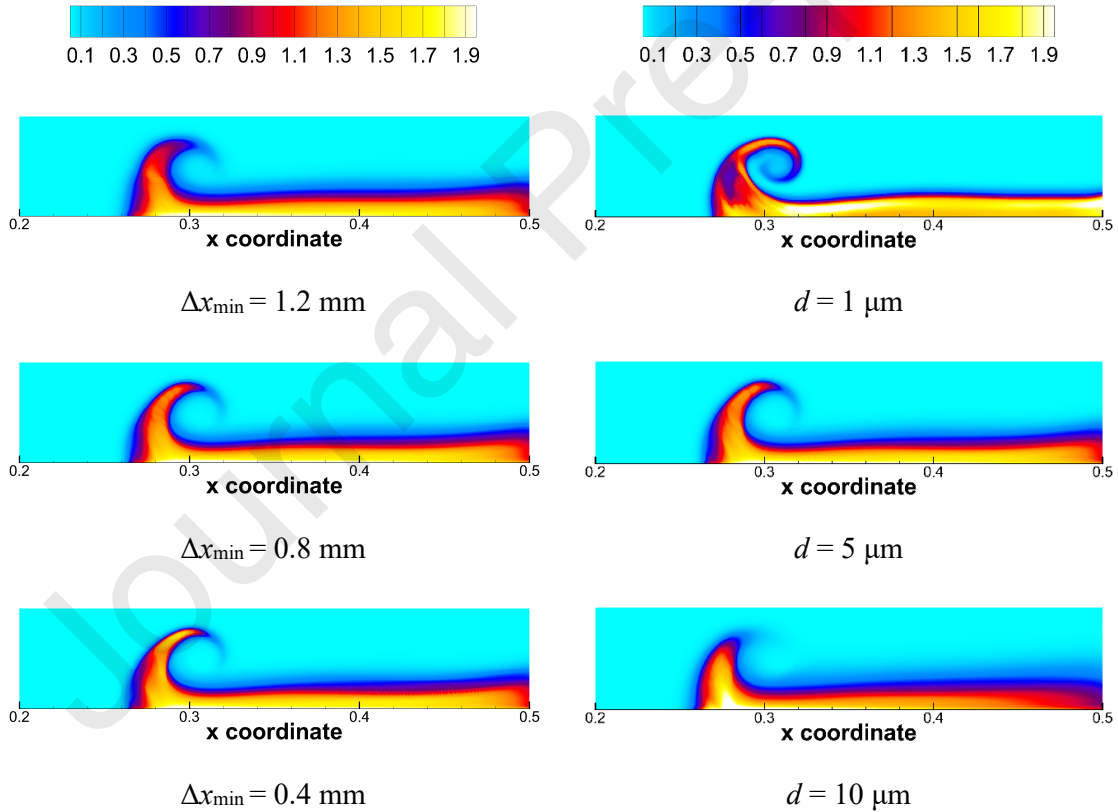


Fig. 7. Contours of concentration of solid phase in the interaction of a shock wave with a dust layer at $t=0.009$ ms: (a) Grid study (left), (b) effect of particle diameters (right).

5.2. Under-expansion of a jet in a dusty environment

To further verify the DG method, we considered the problem of the under-expanded jet, which contains some features of the rocket plume expansion and regolith dispersal in the lunar landing problem. The problem of a supersonic jet expanding from a high-pressure chamber into a low-pressure chamber can be used to verify the first-order Boltzmann-Curtiss-based constitutive relations. **Fig. 8** (a) provides a schematic of the physical features of the under-expanded jet flow. The location of the Mach disk in the absence of particles was first calculated to validate the pure gas solver. This parameter has been experimentally studied by various researchers in the past [104-107]. Recently, Franquet *et al.* [108] presented an extensive review of experimental works on free under-expanded jets.

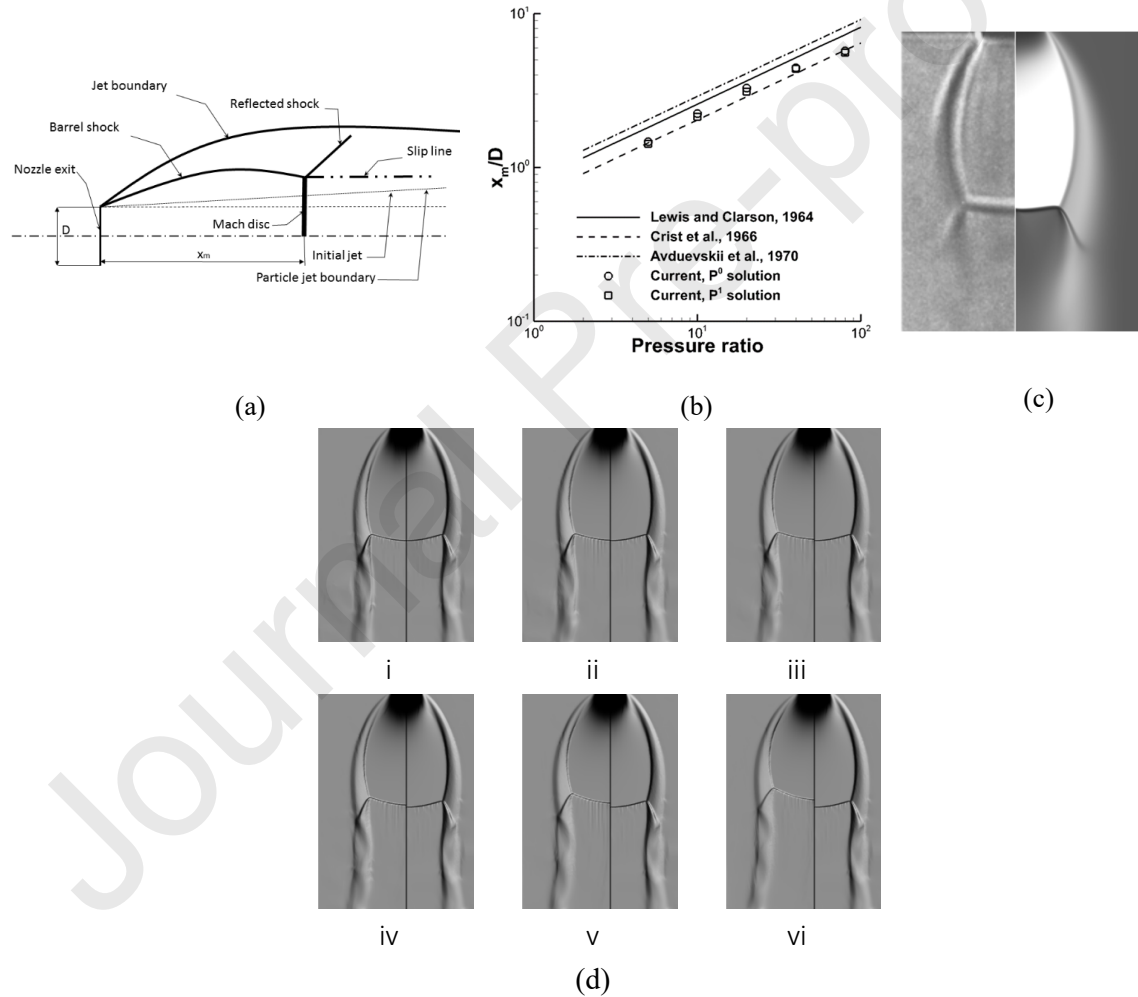


Fig. 8. Verification and validation of the DG solutions in underexpanded jet for pure and dusty gas cases: (a) Schematic of the problem, (b) validation of the Mach disk location for pure gas, (c) a comparison of numerical shadowgraphs with experimental Schlieren image for a pressure ratio of 29.8 in pure gas, (d) upstream movement of the Mach disk location due to the addition of dust particles: **i)** $\beta = 0.0$; **ii)** $\beta = 0.11$; **iii)** $\beta = 0.24$; **iv)** $\beta = 0.35$; **v)** $\beta = 0.64$; **vi)** $\beta = 1.07$ ($P_0 = 0.31\text{MPa}$, $P_0/P_\infty = 29.8$, $d = 45\mu\text{m}$) (P^1 solution)

The comparison of the Mach disk location with experimental results is shown in **Fig. 8** (b). Generally, the results are shown to be in good agreement with the experimental data of Avduevskii *et al.* [107] for mid-range pressure ratios. For pressure ratios of 2 and 100, our predictions were closer to the experimental results of Lewis and Carlson [104]. A comparison of numerical shadowgraphs with experimental Schlieren images for a pressure ratio of 29.8 is also shown in **Fig. 8** (c). Moreover, the effect of the presence of particles on the flow is shown in **Fig. 8** (d). The upstream movement of the Mach disk is apparent in the numerical shadowgraphs which are in accordance with the experimental results from Sommerfeld [106]. Complementary discussions on this topic, including the role of the Stokes number on the counter-intuitive behavior of the Mach disk movement, can be found in our recent work [51].

5.3 Jet impingement on a dusty surface

A schematic of the computational domain and boundary conditions is shown in **Fig. 9** (a). The viscous wall boundary condition was applied to the nozzle wall and lunar surface. The symmetry condition was assigned on the central axis. The chamber condition was imposed on the inlet of the converging-diverging nozzle. On the other boundaries of the domain, the ambient condition of the lunar atmosphere was imposed. A sample computational grid is shown in **Fig. 9** (b). It must be noted that the computational grid should be extended a reasonable distance from the exit jet to minimize the numerical boundary effects on the solution. In our simulations, the domain was extended $20L$ and $10L$ in the horizontal and vertical directions, respectively.

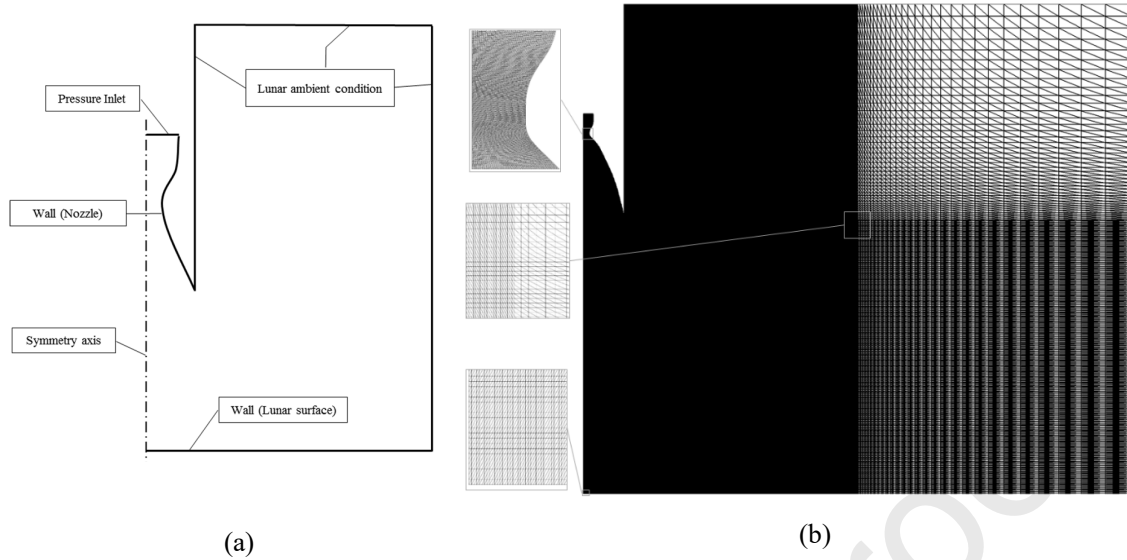


Fig. 9. Schematic of the computational domain: (a) Boundary conditions, (b) a sample computational grid at a hovering altitude of 5 m.

A comparison of the Mach solution with the experimental Schlieren image obtained by Land and Clark [109] is shown in **Fig. 10**. The working gas is assumed to be nitrogen, and the exit Mach number was set to 5. The numerical results show good qualitative agreement with the experimental results in the degree of expansion of plume, shock standoff distance, and general geometrical shape of the plume. For the test cases where the jet impinges on the wall, a shock detection algorithm was activated along with the positivity and monotonicity limiters. The rest of the parameters, such as the flux functions and limiters, were set similar to previous cases.

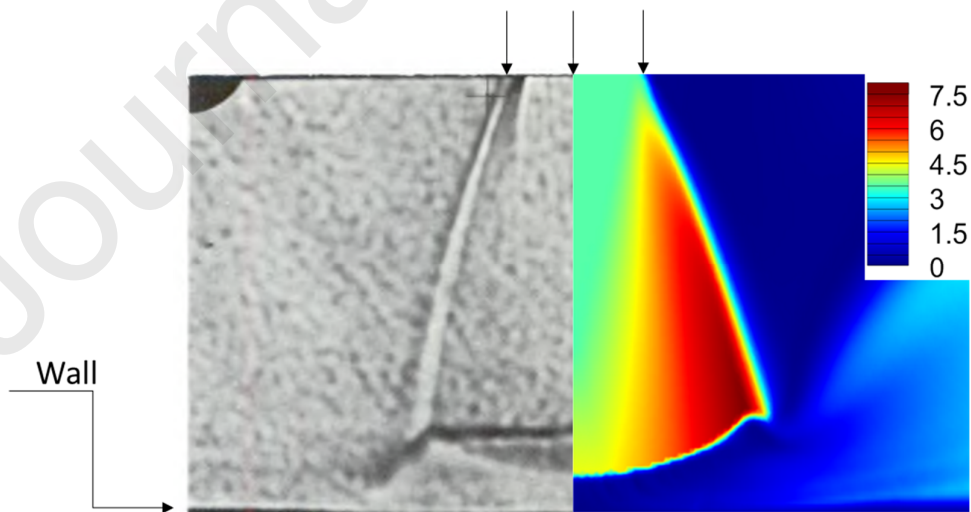


Fig. 10. Comparison of the DG solution of jet impingement on the surface with the experimental result [109] (nitrogen gas, $M=5.0$, $Re=10000$, pressure ratio=3.79, $h/D=6.7$): Mean Schlieren image (left) and DG solution of local Mach number (right).

Because of the technical difficulties involved in performing an actual experiment (vacuum condition, low gravity, etc.), very few experimental studies of this type of problem are available. Even in the available experiments, some assumptions were inevitably made to simplify the problem. Therefore, to further validate the DG method, the results were compared with previous DSMC solutions, specifically the works by Morris [110] in 2010.

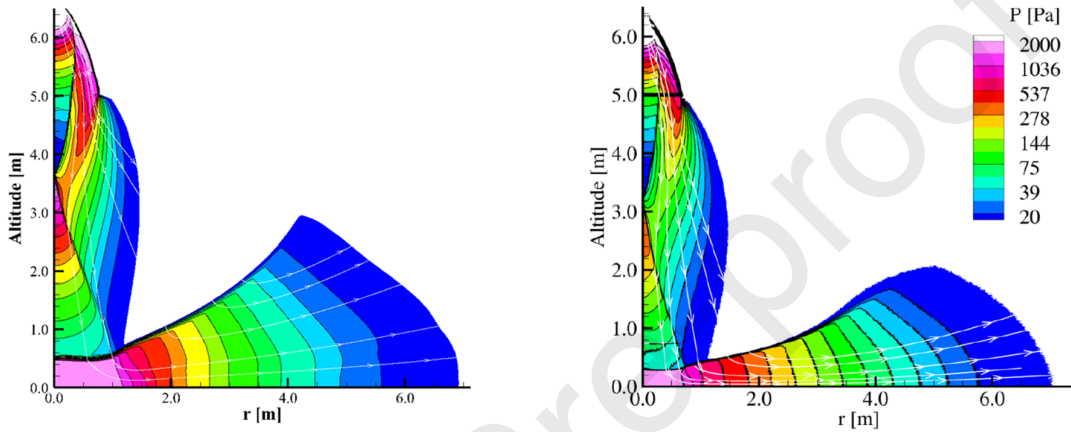


Fig. 11. Comparison of pressure contours (hover altitude 5 m): NCCR (left) and DSMC solution [110] (right). Throat average properties: $M=1.0$, $p=144630$ Pa, $T=2458$ K. Ambient properties: $p=5$ Pa, $T=273$ K. Water vapor with a constant specific heats of 1.3 is used for simulation.

In **Fig. 11**, the pressure solution of the second-order Boltzmann-Curtiss-based nonlinear coupled constitutive relation (NCCR) is compared with the DSMC solution. The DG solutions are in qualitatively good agreement with their DSMC counterparts. However, some deviations can be observed, in the prediction of the height of the normal shock wave and the location of the reflection wave. These deviations may be due to slightly different nozzle profiles or differences in some of the setup parameters related to the inherent gap between the DSMC and continuum theory.

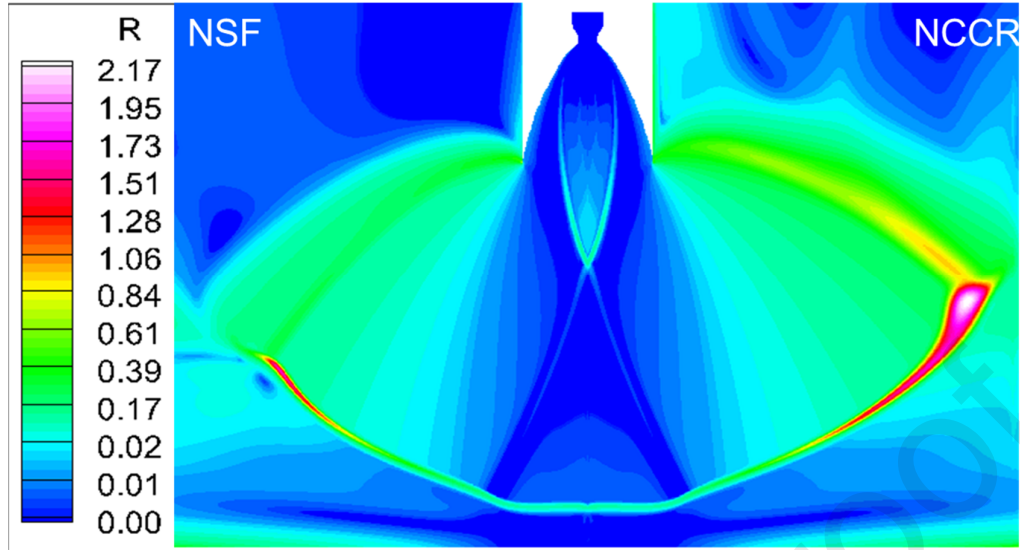


Fig. 12. Comparison of the Rayleigh-Onsager dissipation function for NSF (left) and NCCR (right). Simulated gas and the boundary conditions correspond to that of Fig. 11.

To demonstrate the degree of non-equilibrium, the Rayleigh-Onsager dissipation function [75] is shown in Fig. 12. A higher degree of thermal non-equilibrium is expected for higher hover altitudes, or when the far-field simulation is of main interest. It can be seen that the core plume region and lunar wall proximity are entirely near the thermal equilibrium state—however, the degree of non-equilibrium is high in the stand-off shock region and the shear layer.

One of the critical parameters that affect the structure of the under-expanded jet and impinging under-expanded jet is the ratio of the exit to the ambient pressure. Before simulating the multiphase flow, an analysis of the effect of ambient pressure was conducted, as shown in Fig. 13. As the ambient pressure decreased, the stand-off shock location drew closer to the surface. Also, the radius of the normal shock wave changed substantially. The degree of under-expansion of the jet was also strongly dependent on this parameter. As can be seen in the Mach contours, the lower the ambient pressure, the higher the degree of under-expansion was.

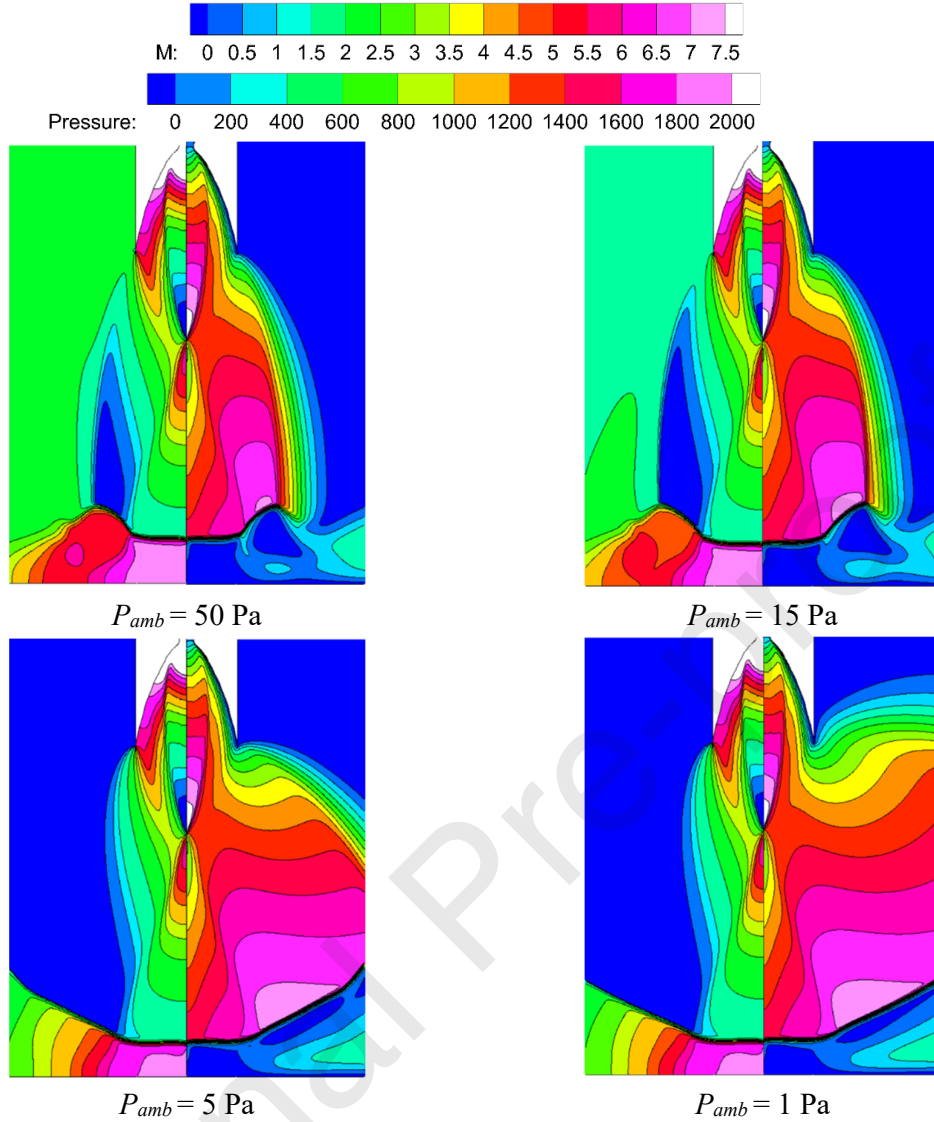


Fig. 13. The effect of ambient pressure on pressure (left) and Mach (right) in the impinging jet. Throat average properties: $M=1.0$, $p=144630 \text{ Pa}$, $T=2458 \text{ K}$. Water vapor with a constant specific heats of 1.3 is used for simulation.

When a simulated jet impingement on a dusty surface includes the nozzle, the flow-field will be more complicated, because of the presence of internal and reflected shocks. These complexities require higher grid resolution, so that the existing physical phenomena can be adequately captured. Moreover, as demonstrated in [110], the effect of the presence of the nozzle on the erosion properties compared to the uniform flow is negligible. A comparison of the number density solutions of NCCR with DPLR and hybrid DPLR-DSMC pressure solutions is shown in **Fig. 14**.

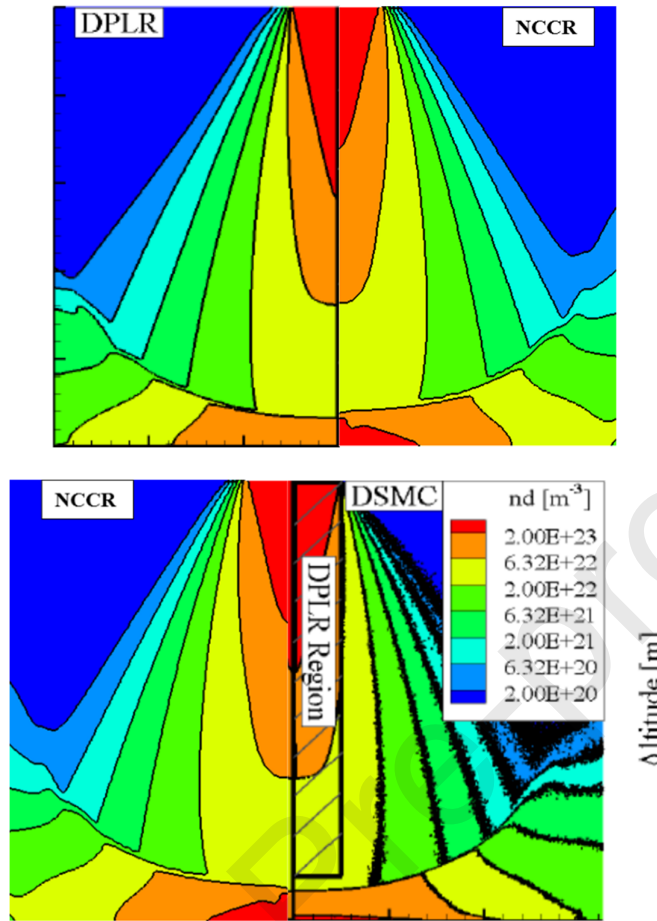


Fig. 14. Comparison of NCCR solution with DPLR and hybrid solutions taken directly from [64]. Exhaust conditions are $M=5$, $T=556\text{K}$. The simulated gas is ammonia.

It can be seen that the NCCR solution is in agreement with both the DSMC solution and the DPLR based on the first-order constitutive relation. Near the surface, the accumulation of particles right under the nozzle is under-predicted by the first-order model. On the other hand, the NCCR model is found to over-predict the area of this range compared to DSMC, while the maximum value of the number density predicted by the NCCR model is in accordance with the DSMC method. Therefore, the present DG solver in conjunction with the second-order NCCR model can improve the quality of the solutions compared with the first-order constitutive model. At the same time, the computational cost and the statistical noise observed in the DSMC solution can be reduced.

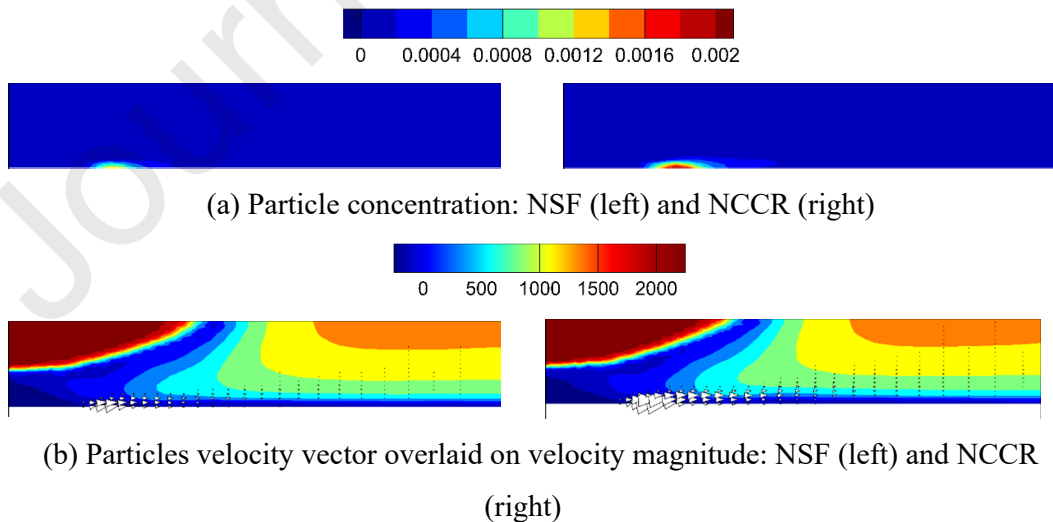
The erosion model in Roberts [58, 64, 110] was shown to be capable of yielding promising results for the erosion rate. However, in the works by Morris [110], when calculating the shear stress exerted on the surface, the dynamic pressure of the gas was measured at a

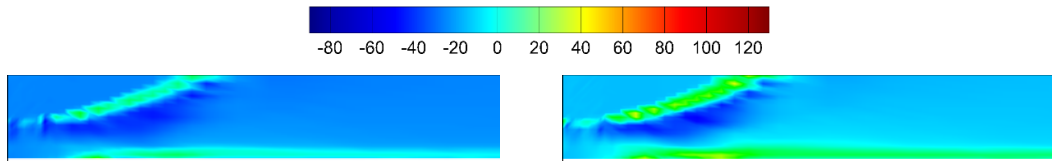
location away from the surface (slightly more than the height of the boundary layer), which is not only physically arguable but also complicates the model implementation in an unstructured algorithm.

In this study, we introduce a more straightforward method in which the excess shear stress is calculated based on the difference between the shear stress of the gas phase on the surface (rather than dynamic pressure) and the critical shear stress for the lunar regolith surface which can be estimated based on the value reported in the literature [111, 112]. In this new model, the coefficient of the soil erosion parameter can be adjusted as a scaling factor. This yielded predictions in agreement with experimental data, as well as with observations gathered from previous lunar missions (for example, Apollo missions).

It should be noted that the main interest of the present study was to develop a general computational strategy for handling a rarefied gas in the presence of solid particles, rather than accurate erosion modeling. Nonetheless, these simple erosion models exhibit satisfactory results when applied in the present framework. However, when more sophisticated erosion mechanisms are needed, further studies based on microscopic modeling (e.g., MD or DEM) will be required in order to provide the adjustable parameters which will be used in the erosion modules of continuum theory.

Furthermore, it is worth noting that when such a sophisticated erosion model is used, the second-order constitutive relations may take on a more important role. This is because the shear stress of the gas on the surface and the mass flow rate of the eroded particles in the erosion model are significantly influenced by non-equilibrium effects.





(c) Shear stress: NSF (left) and NCCR (right)

Fig. 15. Comparison of first-order and second-order constitutive relations in the erosion modeling: (a) Particle concentration, (b) solid phase velocity vector overlaid on vertical velocity, (c) shear stress.

In **Fig. 15**, the contours of particle concentration, the solid phase velocity vector overlaid on vertical velocity, and shear stress are compared for the NSF and NCCR solutions. It shows how the different constitutive models affect the estimation of the mass of eroded particles that are ejected into the flowfield. The concentration and the velocity of the eroded particles on the surface predicted by the NCCR model are shown in general to be higher than those of the NSF prediction. This is because the NCCR model provides a better estimation of the constitutive parameters when the degree of non-equilibrium is high.

6. Concluding remarks

We have presented a novel computational strategy for solving dusty gas flow problems in non-equilibrium flow conditions within a full continuum framework. The method can be applied to a broad spectrum of gas and solid regimes as long as the fundamental assumptions of the two-fluid models are not violated. An important and yet very challenging problem is the plume-surface interaction and regolith erosion and dispersal during lunar landing, where an underexpanded jet impinges on a dusty bed, and consequent surface erosion leads to a dispersion of particles into an almost vacuum environment.

Even though discrete modeling methods like the DSMC method have shown excellent performance when simulating high Knudsen and high Mach number gas flows, the computational cost of these methods is still high when dealing with near continuum flow regimes. Therefore, in complex flow problems where a variety of regimes co-exist (including the lunar landing problem), a unified flow solver is necessary.

A modal discontinuous Galerkin method was developed based on the second-order Boltzmann-Curtiss-based constitutive relations, for solving the two-fluid system of equations for dusty gases in rarefied condition. The developed DG scheme not only meets the requirement of the positivity/monotonicity preserving property for accurately simulating dusty/granular gas flows, but it can also efficiently handle the numerically problematic source

terms, without resorting to the operator splitting method commonly used in the conventional finite volume method.

Moreover, a simple and yet very effective approach to treat the non-strictly hyperbolic pressureless Euler equations was developed, enabling the straightforward application of the existing inviscid Euler flux functions. This eliminates the need to develop schemes that are specific only to the equations of the solid phase. Regarding the viscous flux, our numerical experiments revealed that, when the Euler-granular model is used, using the BR1 scheme makes the numerical process unstable and leads to instant divergence, while the LDG method can quickly remedy the stability problem.

The problem of a shock wave interacting with a loose dust layer was studied to verify the new constitutive relations that were used for the solid phase. A comparison was made between the zeroth-order Euler-Euler model and the second-order Euler-granular model. An analysis was also conducted of the effect of particle diameter on the topology of the dust layer after interaction with the shock wave.

To further validate the DG solutions, the problems of a free under-expanded jet and jet impingement on a dusty surface were studied. The simulation results were in good agreement with the experimental data in both cases. Lastly, for the case of jet impingement on a dusty surface in the rarefied lunar condition, the present second-order DG solution was shown to be in better agreement with the DSMC solution than the DPLR based on the first-order constitutive relation, specifically near the surface, where the accumulation of particles right under the nozzle was under-predicted by the first-order model.

It should be noted that, near the lunar surface, even the first-order NF or NSF constitutive relations can provide acceptable solutions, since the degree of rarefaction in the core of the plume is not high. However, if a far-field simulation is of interest, the first-order models would considerably deviate from correct solutions. Therefore, second-order constitutive relations for the gas phase will remain essential in the study of far-field flow fields and the free-molecular trajectory of dust particles in the surrounding. Developing more accurate erosion models and second-order Boltzmann-based constitutive relations for the solid phase using the method of moments remain important topics for future study.

Acknowledgments

This work was supported by the National Research Foundation of Korea (NRF 2017-R1A5A1015311 and 2017-R1A2B2007634), South Korea. The first author (O.E.)

acknowledges the support provided by the Korea Institute of Science and Technology Information (KISTI), South Korea.

References

- [1] H. Miura, I.I. Glass, On a dusty-gas shock tube, in: *Proceedings of the Royal Society of London A: Mathematical, Physical and Engineering Sciences*, The Royal Society, 1982, pp. 373-388.
- [2] O. Igra, G. Ben-Dor, Z. Rakib, The effect of dust and water droplets on the relaxation zone developed behind strong normal shock waves, *International Journal of Multiphase Flow*, 11 (1985) 121-132.
- [3] I. Toumi, A. Kumbaro, An approximate linearized Riemann solver for a two-fluid model, *Journal of Computational Physics*, 124 (1996) 286-300.
- [4] I. Tiselj, S. Petelin, Modelling of two-phase flow with second-order accurate scheme, *Journal of Computational Physics*, 136 (1997) 503-521.
- [5] L. Sainsaulieu, Finite volume approximation of two phase-fluid flows based on an approximate Roe-type Riemann solver, *Journal of Computational Physics*, 121 (1995) 1-28.
- [6] O. Igra, I. Elperin, G. Ben-Dor, Dusty gas flow in a converging-diverging nozzle, *Journal of Fluids Engineering*, 121 (1999) 908-913.
- [7] T. Saito, Numerical analysis of dusty-gas flows, *Journal of Computational Physics*, 176 (2002) 129-144.
- [8] T. Saito, M. Marumoto, K. Takayama, Numerical investigations of shock waves in gas-particle mixtures, *Shock Waves*, 13 (2003) 299-322.
- [9] M. Pelanti, R.J. LeVeque, High-resolution finite volume methods for dusty gas jets and plumes, *SIAM Journal on Scientific Computing*, 28 (2006) 1335-1360.
- [10] A. Vić, H. Pouransari, R. Zamansky, A. Mani, Particle-laden flows forced by the disperse phase: Comparison between Lagrangian and Eulerian simulations, *International Journal of Multiphase Flow*, 79 (2016) 144-158.
- [11] M.A. van der Hoef, M. Ye, M. van Sint Annaland, A.T. Andrews, S. Sundaresan, J.A.M. Kuipers, Multiscale Modeling of Gas-Fluidized Beds, *Advances in Chemical Engineering*, 31 (2006) 65-149.
- [12] T.B. Anderson, R. Jackson, Fluid mechanical description of fluidized beds. Equations of motion, *Industrial & Engineering Chemistry Fundamentals*, 6 (1967) 527-539.
- [13] Y.P. Tsuo, D. Gidaspow, Computation of flow patterns in circulating fluidized beds, *AIChE Journal*, 36 (1990) 885-896.
- [14] J. Kuipers, K. Van Duin, F. Van Beckum, W.P.M. Van Swaaij, A numerical model of gas-fluidized beds, *Chemical Engineering Science*, 47 (1992) 1913-1924.
- [15] C. Lun, S.B. Savage, D. Jeffrey, N. Chepurniy, Kinetic theories for granular flow: inelastic particles in Couette flow and slightly inelastic particles in a general flowfield, *Journal of Fluid Mechanics*, 140 (1984) 223-256.
- [16] M. Reeks, On the constitutive relations for dispersed particles in nonuniform flows. I: Dispersion in a simple shear flow, *Physics of Fluids A: Fluid Dynamics*, 5 (1993) 750-761.
- [17] D. Gidaspow, *Multiphase flow and fluidization: continuum and kinetic theory descriptions*, Academic Press, 1994.
- [18] J.A. Gantt, E.P. Gatzke, Kinetic theory of granular flow limitations for modeling high-shear mixing, *Industrial & Engineering Chemistry Research*, 45 (2006) 6721-6727.
- [19] S. Schneiderbauer, A. Aigner, S. Pirker, A comprehensive frictional-kinetic model for gas-particle flows: Analysis of fluidized and moving bed regimes, *Chemical Engineering Science*, 80 (2012) 279-292.

- [20] R.W. Houim, E.S. Oran, A multiphase model for compressible granular-gaseous flows: formulation and initial tests, *Journal of Fluid Mechanics*, 789 (2016) 166-220.
- [21] A. Busch, S.T. Johansen, On the validity of the two-fluid-KTGF approach for dense gravity-driven granular flows, *Powder Technology*, (2020).
- [22] O. Desjardins, R.O. Fox, P. Villedieu, A quadrature-based moment method for dilute fluid-particle flows, *Journal of Computational Physics*, 227 (2008) 2514-2539.
- [23] R.O. Fox, Higher-order quadrature-based moment methods for kinetic equations, *Journal of Computational Physics*, 228 (2009) 7771-7791.
- [24] M. Sabat, A. Larat, A. Vié, M. Massot, On the development of high order realizable schemes for the Eulerian simulation of disperse phase flows on unstructured grids: a convex-state preserving discontinuous Galerkin method, *The Journal of Computational Multiphase Flows*, 6(3) (2014) 247-270.
- [25] C. Liu, Z. Wang, K. Xu, A unified gas-kinetic scheme for continuum and rarefied flows VI: Dilute disperse gas-particle multiphase system, *Journal of Computational Physics*, 386 (2019) 264-295.
- [26] P.T. Metzger, J. Smith, J.E. Lane, Phenomenology of soil erosion due to rocket exhaust on the Moon and the Mauna Kea lunar test site, *Journal of Geophysical Research: Planets*, 116 (2011).
- [27] A. Gorman, *Dr Space Junk vs The Universe: Archaeology and the Future*, NewSouth, 2019.
- [28] O. Abouali, S. Saadabadi, H. Emdad, Numerical investigation of the flow field and cut-off characteristics of supersonic/hypersonic impactors, *Journal of Aerosol Science*, 42 (2011) 65-77.
- [29] C.W. Shu, Discontinuous Galerkin methods for time-dependent convection dominated problems: Basics, recent developments and comparison with other methods, in: *Building Bridges: Connections and Challenges in Modern Approaches to Numerical Partial Differential Equations*, Springer, 2016, pp. 371-399.
- [30] F. Bassi, S. Rebay, A high-order accurate discontinuous finite element method for the numerical solution of the compressible Navier-Stokes equations, *Journal of Computational Physics*, 131 (1997) 267-279.
- [31] B. Cockburn, C.W. Shu, The Runge-Kutta discontinuous Galerkin method for conservation laws V: multidimensional systems, *Journal of Computational Physics*, 141 (1998) 199-224.
- [32] K. Kontzialis, J.A. Ekaterinaris, High order discontinuous Galerkin discretizations with a new limiting approach and positivity preservation for strong moving shocks, *Computers & Fluids*, 71 (2013) 98-112.
- [33] H. You, C. Kim, Direct reconstruction method for discontinuous Galerkin methods on higher-order mixed-curved meshes I. Volume integration, *Journal of Computational Physics*, 395 (2019) 223-246.
- [34] F.X. Giraldo, T. Warburton, A high-order triangular discontinuous Galerkin oceanic shallow water model, *International journal for numerical methods in fluids*, 56 (2008) 899-925.
- [35] J. Iannelli, An implicit Galerkin finite element Runge-Kutta algorithm for shock-structure investigations, *Journal of Computational Physics*, 230 (2011) 260-286.
- [36] L. Li, Q. Zhang, A new vertex-based limiting approach for nodal discontinuous Galerkin methods on arbitrary unstructured meshes, *Computers & Fluids*, 159 (2017) 316-326.
- [37] W. Boscheri, D.S. Balsara, High order direct Arbitrary-Lagrangian-Eulerian (ALE) PNPM schemes with WENO Adaptive-Order reconstruction on unstructured meshes, *Journal of Computational Physics*, 398 (2019) 108899.
- [38] B. Cockburn, G.E. Karniadakis, C.W. Shu, The development of discontinuous Galerkin methods, in: *Discontinuous Galerkin Methods*, Springer, 2000, pp. 3-50.
- [39] B. Rivière, M.F. Wheeler, V. Girault, Improved energy estimates for interior penalty, constrained and discontinuous Galerkin methods for elliptic problems. Part I, *Computational Geosciences*, 3 (1999) 337-360.

- [40] S. Sun, M.F. Wheeler, Discontinuous Galerkin methods for coupled flow and reactive transport problems, *Applied Numerical Mathematics*, 52 (2005) 273-298.
- [41] W. Klieber, B. Rivière, Adaptive simulations of two-phase flow by discontinuous Galerkin methods, *Computer Methods in Applied Mechanics and Engineering*, 196 (2006) 404-419.
- [42] M. Owkes, O. Desjardins, A discontinuous Galerkin conservative level set scheme for interface capturing in multiphase flows, *Journal of Computational Physics*, 249 (2013) 275-302.
- [43] D. Diehl, J. Kremser, D. Kröner, C. Rohde, Numerical solution of Navier–Stokes–Korteweg systems by local discontinuous Galerkin methods in multiple space dimensions, *Applied Mathematics and Computation*, 272 (2016) 309-335.
- [44] M. Dumbser, R. Loubère, A simple robust and accurate a posteriori sub-cell finite volume limiter for the discontinuous Galerkin method on unstructured meshes, *Journal of Computational Physics*, 319 (2016) 163-199.
- [45] J. Moortgat, A. Firoozabadi, Mixed-hybrid and vertex-discontinuous-Galerkin finite element modeling of multiphase compositional flow on 3D unstructured grids, *Journal of Computational Physics*, 315 (2016) 476-500.
- [46] N.T.P. Le, H. Xiao, R.S. Myong, A triangular discontinuous Galerkin method for non-Newtonian implicit constitutive models of rarefied and microscale gases, *Journal of Computational Physics*, 273 (2014) 160-184.
- [47] H. Xiao, R.S. Myong, Computational simulations of microscale shock–vortex interaction using a mixed discontinuous Galerkin method, *Computers & Fluids*, 105 (2014) 179-193.
- [48] L.P. Raj, S. Singh, A. Karchani, R.S. Myong, A super-parallel mixed explicit discontinuous Galerkin method for the second-order Boltzmann-based constitutive models of rarefied and microscale gases, *Computers & Fluids*, 157 (2017) 146-163.
- [49] S. Singh, A. Karchani, R.S. Myong, Non-equilibrium effects of diatomic and polyatomic gases on the shock-vortex interaction based on the second-order constitutive model of the Boltzmann-Curtiss equation, *Physics of Fluids*, 30 (2018) 016109.
- [50] O. Ejtehadi, A. Rahimi, A. Karchani, R.S. Myong, Complex wave patterns in dilute gas–particle flows based on a novel discontinuous Galerkin scheme, *International Journal of Multiphase Flow*, 104 (2018) 125-151.
- [51] O. Ejtehadi, A. Rahimi, R.S. Myong, Numerical investigation of the counter-intuitive behavior of Mach disk movement in underexpanded gas-particle jets, *Journal of Computational Fluid Engineering*, 24 (2019) 19-28.
- [52] R.S. Myong, A computational method for Eu's generalized hydrodynamic equations of rarefied and microscale gasdynamics, *Journal of Computational Physics*, 168 (2001) 47-72.
- [53] R.S. Myong, A generalized hydrodynamic computational model for rarefied and microscale diatomic gas flows, *Journal of Computational Physics*, 195 (2004) 655-676.
- [54] R.S. Myong, Numerical simulation of hypersonic rarefied flows using the second-order constitutive model of the Boltzmann equation, in: *Advances in Some Hypersonic Vehicles Technologies*, InTech, 2018.
- [55] A. Rana, R. Ravichandran, J. Park, R.S. Myong, Microscopic molecular dynamics characterization of the second-order non-Navier-Fourier constitutive laws in the Poiseuille gas flow, *Physics of Fluids*, 28 (2016) 082003.
- [56] T.J. Stubbs, R.R. Vondrak, W.M. Farrell, Impact of dust on lunar exploration, URL: <http://hefd.jsc.nasa.gov/files/StubbsImpactOnExploration>, 4075 (2007).
- [57] X. He, B. He, G. Cai, Simulation of rocket plume and lunar dust using DSMC method, *Acta Astronautica*, 70 (2012) 100-111.
- [58] A. Morris, D. Goldstein, P. Varghese, L. Trafton, Modeling the interaction between a rocket plume, scoured regolith, and a plume deflection fence, in: *Earth and Space 2012: Engineering, Science, Construction, and Operations in Challenging Environments*, 2012, pp. 189-198.

- [59] A.B. Morris, D.B. Goldstein, P.L. Varghese, L.M. Trafton, Approach for modeling rocket plume impingement and dust dispersal on the moon, *Journal of Spacecraft and Rockets*, 52 (2015) 362-374.
- [60] J. Burt, I. Boyd, Development of a two-way coupled model for two phase rarefied flows, in: 42nd AIAA Aerospace Sciences Meeting and Exhibit, 2004, pp. 1351.
- [61] M. Gallis, J. Torczynski, D. Rader, An approach for simulating the transport of spherical particles in a rarefied gas flow via the direct simulation Monte Carlo method, *Physics of Fluids*, 13 (2001) 3482-3492.
- [62] S. Gimelshein, A. Alexeenko, D. Wadsworth, N. Gimelshein, The influence of particulates on thruster plume/shock layer interaction at high altitudes, in: 43rd AIAA Aerospace Sciences Meeting and Exhibit, 2004, pp. 766.
- [63] D. Liu, S. Yang, Z. Wang, H. Liu, C. Cai, D. Wu, On rocket plume, lunar crater and lunar dust interactions, in: 48th AIAA Aerospace Sciences Meeting Including the New Horizons Forum and Aerospace Exposition, 2010, pp. 1161.
- [64] A. Morris, D. Goldstein, P. Varghese, L. Trafton, Plume impingement on a dusty lunar surface, in: AIP Conference Proceedings, AIP, 2011, pp. 1187-1192.
- [65] M.J. Wright, G.V. Candler, D. Bose, Data-parallel line relaxation method for the Navier-Stokes equations, *AIAA Journal*, 36 (1998) 1603-1609.
- [66] A. Rahimi, O. Ejtehadi, K.H. Lee, R.S. Myong, Near-field plume-surface interaction and regolith erosion and dispersal during the lunar landing, In Review.
- [67] R. Ishii, Y. Umeda, M. Yuhi, Numerical analysis of gas-particle two-phase flows, *Journal of Fluid Mechanics*, 203 (1989) 475-515.
- [68] S.W. Kim, K.S. Chang, Reflection of shock wave from a compression corner in a particle-laden gas region, *Shock Waves*, 1 (1991) 65-73.
- [69] O. Igra, G. Hu, J. Falcovitz, B. Wang, Shock wave reflection from a wedge in a dusty gas, *International Journal of Multiphase Flow*, 30 (2004) 1139-1169.
- [70] C. Curtiss, The classical Boltzmann equation of a gas of diatomic molecules, *The Journal of Chemical Physics*, 75 (1981) 376-378.
- [71] R.S. Myong, Coupled nonlinear constitutive models for rarefied and microscale gas flows: subtle interplay of kinematics and dissipation effects, *Continuum Mechanics and Thermodynamics*, 21 (2009) 389-399.
- [72] R.S. Myong, On the high Mach number shock structure singularity caused by overreach of Maxwellian molecules, *Physics of Fluids*, 26 (2014) 056102.
- [73] B.C. Eu, *Kinetic theory and irreversible thermodynamics*, John Wiley and Sons, Inc., 1992.
- [74] B.C. Eu, Y.G. Ohr, Generalized hydrodynamics, bulk viscosity, and sound wave absorption and dispersion in dilute rigid molecular gases, *Physics of Fluids*, 13 (2001) 744-753.
- [75] L. Onsager, Reciprocal relations in irreversible processes. I, *Physical review*, 37 (1931) 405.
- [76] S. Chapman, T.G. Cowling, *The mathematical theory of non-uniform gases: an account of the kinetic theory of viscosity, thermal conduction and diffusion in gases*, Cambridge university press, 1970.
- [77] J.P. Hansen, I.R. McDonald, *Theory of simple liquids*, Elsevier, 1990.
- [78] N.F. Carnahan, K.E. Starling, Equation of state for nonattracting rigid spheres, *The Journal of Chemical Physics*, 51 (1969) 635.
- [79] D. Ma, G. Ahmadi, An equation of state for dense rigid sphere gases, *The Journal of Chemical Physics*, 84 (1986) 3449-3450.
- [80] Y. Song, E. Mason, R.M. Stratt, Why does the Carnahan-Starling equation work so well?, *The Journal of Physical Chemistry*, 93 (1989) 6916-6919.
- [81] B. Alder, T. Wainwright, Phase transition in elastic disks, *Physical Review*, 127 (1962) 359.

- [82] L. Woodcock, LV Woodcock, *Ann. NY Acad. Sci.* 371, 274 (1981), *Ann. NY Acad. Sci.*, 371 (1981) 274.
- [83] W.H. Reed, T.R. Hill, Triangular mesh methods for the neutron transport equation, in: Technical Report LA-UR-73-479, Los Alamos Scientific Lab., N. Mex. (USA), 1973.
- [84] B. Cockburn, C.W. Shu, The Runge-Kutta local projection P^1 -discontinuous-Galerkin finite element method for scalar conservation laws, *Rairo-Modélisation Mathématique et Analyse Numérique*, 25 (1988) 337-361.
- [85] B. Cockburn, C.W. Shu, TVB Runge-Kutta local projection discontinuous Galerkin finite element method for conservation laws. II. General framework, *Mathematics of Computation*, 52 (1989) 411-435.
- [86] M. Dubiner, Spectral methods on triangles and other domains, *Journal of Scientific Computing*, 6 (1991) 345-390.
- [87] V.V.e. Rusanov, Calculation of interaction of non-steady shock waves with obstacles, NRC, Division of Mechanical Engineering, 1962.
- [88] H. Nishikawa, K. Kitamura, Very simple, carbuncle-free, boundary-layer-resolving, rotated-hybrid Riemann solvers, *Journal of Computational Physics*, 227 (2008) 2560-2581.
- [89] M.S. Liou, C.J. Steffen Jr, A new flux splitting scheme, *Journal of Computational Physics*, 107 (1993) 23-39.
- [90] M.S. Liou, A sequel to AUSM, Part II: AUSM+_{up} for all speeds, *Journal of Computational Physics*, 214 (2006) 137-170.
- [91] D.N. Arnold, F. Brezzi, B. Cockburn, D. Marini, Discontinuous Galerkin methods for elliptic problems, in: *Discontinuous Galerkin Methods*, Springer, 2000, pp. 89-101.
- [92] D.N. Arnold, F. Brezzi, B. Cockburn, L.D. Marini, Unified analysis of discontinuous Galerkin methods for elliptic problems, *SIAM Journal on Numerical Analysis*, 39 (2002) 1749-1779.
- [93] B. Cockburn, C.-W. Shu, The local discontinuous Galerkin method for time-dependent convection-diffusion systems, *SIAM Journal on Numerical Analysis*, 35 (1998) 2440-2463.
- [94] E. Toro, Riemann-problem-based techniques for computing reactive two-phased flows, in: *Numerical Combustion*, Springer, 1989, pp. 472-481.
- [95] R. Saurel, R. Abgrall, A multiphase Godunov method for compressible multifluid and multiphase flows, *Journal of Computational Physics*, 150 (1999) 425-467.
- [96] K. Powell, P. Roe, R.S. Myong, T. Gombosi, An upwind scheme for magnetohydrodynamics, in: *12th Computational Fluid Dynamics Conference*, 1995, pp. 1704.
- [97] K.G. Powell, P.L. Roe, T.J. Linde, T.I. Gombosi, D.L. De Zeeuw, A solution-adaptive upwind scheme for ideal magnetohydrodynamics, *Journal of Computational Physics*, 154 (1999) 284-309.
- [98] P. Janhunen, A positive conservative method for magnetohydrodynamics based on HLL and Roe methods, *Journal of Computational Physics*, 160 (2000) 649-661.
- [99] S. Jung, R.S. Myong, A second-order positivity-preserving finite volume upwind scheme for air-mixed droplet flow in atmospheric icing, *Computers & Fluids*, 86 (2013) 459-469.
- [100] X. Zhang, C.W. Shu, Positivity-preserving high order discontinuous Galerkin schemes for compressible Euler equations with source terms, *Journal of Computational Physics*, 230 (2011) 1238-1248.
- [101] X. Zhang, C.W. Shu, On maximum-principle-satisfying high order schemes for scalar conservation laws, *Journal of Computational Physics*, 229 (2010) 3091-3120.
- [102] T.J. Barth, D.C. Jespersen, The design and application of upwind schemes on unstructured meshes, in: *27th Aerospace Sciences Meeting*, American Institute of Aeronautics and Astronautics, 1989.
- [103] A. Fedorov, Y.V. Kharlamova, Reflection of a shock wave in a dusty cloud, *Combustion, Explosion, and Shock Waves*, 43 (2007) 104-113.

- [104] C. Lewis, D. Carlson, Normal shock location in underexpanded gas and gas-particle jets, *AIAA Journal*, 2 (1964) 776-777.
- [105] S. Crist, D. Glass, P. Sherman, Study of the highly underexpanded sonic jet, *AIAA Journal*, 4 (1966) 68-71.
- [106] M. Sommerfeld, The structure of particle-laden, underexpanded free jets, *Shock Waves*, 3 (1994) 299-311.
- [107] V.S. Avduevskii, A. Ivanov, I.M. Karpman, V.D. Traskovskii, M.Y. Yudelovich, Flow in supersonic viscous under expanded jet, *Fluid Dynamics*, 5 (1970) 409-414.
- [108] E. Franquet, V. Perrier, S. Gibout, P. Bruel, Free underexpanded jets in a quiescent medium: a review, *Progress in Aerospace Sciences*, 77 (2015) 25-53.
- [109] N.S. Land, L.V. Clark, Experimental investigation of jet impingement on surfaces of fine particles in a vacuum environment, National Aeronautics and Space Administration, 1965.
- [110] A.B. Morris, Simulation of rocket plume impingement and dust dispersal on the lunar surface, in, The University of Texas at Austin, 2012.
- [111] J. Mitchell, W. Houston, R. Scott, N. Costes, W. Carrier III, L. Bromwell, Mechanical properties of lunar soil: Density, porosity, cohesion and angle of internal friction, in: *Lunar and Planetary Science Conference Proceedings*, 1972, pp. 3235.
- [112] J. Colwell, S. Batiste, M. Horányi, S. Robertson, S. Sture, Lunar surface: Dust dynamics and regolith mechanics, *Reviews of Geophysics*, 45 (2007).

Declaration of interests

The authors declare that they have no known competing financial interests or personal relationships that could have appeared to influence the work reported in this paper.

The authors declare the following financial interests/personal relationships which may be considered as potential competing interests:

Journal Pre-proof